DOI: 10.1002/ (aenm.201801280)
Article type: Full Paper

A Porphyrin/Graphene Framework: A Highly Efficient and Robust Electrocatalyst for Carbon Dioxide Reduction

Jaecheol Choi, Pawel Wagner, Rouhollah Jalili, Jeonghun Kim, Douglas R. MacFarlane, Gordon G. Wallace, and David L. Officer**

J. Choi, Dr. P. Wagner, Dr. R. Jalili, Prof. G. G. Wallace, Prof. D. L. Officer
ARC Centre of Excellence for Electromaterials Science and the Intelligent Polymer Research Institute, University of Wollongong, Wollongong, NSW, 2522, Australia
E-mail: davido@uow.edu.au, gwallace@uow.edu.au.

Dr. R. Jalili
School of Science, RMIT University, Melbourne, VIC 3000, Australia

Dr. J. Kim
Institute for Superconducting & Electronic Materials, University of Wollongong, Wollongong, NSW, 2522, Australia

Prof. D. R. MacFarlane
ARC Centre of Excellence for Electromaterials Science, Monash University, Clayton, VIC, 3800, Australia

Keywords: electrochemical CO_2 reduction, heterogeneous catalyst, water-soluble porphyrin, graphene framework

Developing immobilized molecular complexes, which demonstrate high product efficiencies at low overpotential in the electrochemical reduction of CO_2 in aqueous media, is essential for the practical production of reduction products. In this work, we demonstrate a simple and facile self-assembly method by electrostatic interaction and π-π stacking for the fabrication of a porphyrin/graphene framework (FePGF) composed of Fe(III)-tetraphenyltrimethyl ammonium porphyrin (FeTMAP) and reduced liquid crystalline graphene oxide (*r*LCGO) that can be utilized for the electrocatalytic reduction of CO_2 to CO on a glassy carbon electrode in aqueous electrolyte. The FePGF results in an outstandingly robust catalytic performance for the production of CO with 97.0% faradaic efficiency at an overpotential of 480 mV and

superior long-term stability relative to other heterogeneous molecular complexes of over 24 h (cathodic energy efficiency: 58.1 %). In addition, a high surface area carbon fiber paper is used as a substrate for FePGF catalyst, resulting in enhanced current density of 1.68 mA cm^{-2} with 98.7 % CO faradaic efficiency at an overpotential of 430 mV for 10 h, corresponding to a TOF of 2.9 s^{-1} and 104,400 TON. Furthermore, FePGF/CFP has one of the highest cathodic energy efficiencies (60.9 %) reported for immobilized metal complex catalysts.

1. Introduction

The increasing atmospheric and marine CO_2 concentrations is widely considered as one of the biggest global issues amongst all environmental problems and managing the emission of CO_2 using renewable energy sources is one of the most important scientific and economic challenges today.[1] As a promising approach to this, the conversion of CO_2 into fuels and organic feedstock materials has been widely investigated using various methods such as thermo-, photo-, and electro-chemical methods.[2] Among them, electrochemical CO_2 reduction converts CO_2 that is dissolved in an aqueous electrolyte into other value-added chemicals (i.e. carbon monoxide, formic acid, alcohols, etc.) using electrical energy and it is one of the most attractive reduction methods due to its environmental and economic advantages.[3] In the overall process in the electrochemical cell, the CO_2 reduction at the cathode is carried out along with water oxidation at the anode. Once each reaction is efficiently optimized, both of reactions can be integrated into the one electrochemical device.

However, there are kinetic challenges in splitting CO_2 molecules due to the high activation energy required in the reduction process.[4] In order to resolve this, a variety of catalysts including precious metals,[5] non-precious metals,[6] transition metal oxide,[6a, 7] transition metal chalcogenides[8] and metal complexes[8b, 9] have been investigated to reduce the activation energy. In the presence of molecular catalysts, specifically, CO_2 reduction typically proceeds

by a proton-coupled electron transfer reaction, resulting in lower overpotentials due to the stabilization of the metal-carbon dioxide complex.[10] Depending on the process under the CO_2 atmosphere, a variety of gaseous or liquid products can be generated at various potentials estimated from the standard Gibbs energies of the reactants.[11] However, the competitive hydrogen evolution reaction (HER, E^0= 0 V vs. RHE)[4] can concomitantly occur at a similar potential to the electrochemical CO_2 reduction reaction.[12] Therefore selectivity is a vital property in a practical electrocatalyst for this process.

Metal complexes (e.g. metalloporphyrins and metallophthalocyanines) have been widely studied as homogeneous catalysts for electrochemical CO_2 reduction due to their high selectivity, potential low cost, and ease of preparation on a large scale.[13] However, the use of the metal complexes as homogeneous catalysts is not ideal for practical applications since the catalytic activities are influenced by a number of factors including (i) diffusion of the catalyst into the diffusion layer adjacent to the electrode surface, limiting the number of active catalytic species, (ii) the difficulty of preventing catalyst deactivation processes such as dimerization and aggregation and (iii) non-ideal use of volatile and flammable organic solvents like dimethylformamide (DMF) and acetonitrile.[14] In addition, unlike heterogeneous catalysts, it is not easy to separate or reuse the homogeneous catalysts following the reaction, one of the most important factors in commercial use.[14]

For these reasons, there have been a number of studies recently in which earth-abundant cobalt, iron and zinc-based molecular complexes have been immobilized and used as heterogeneous catalysts for electrochemical CO_2 reduction.[15] For example, a cobalt-based heterogeneous catalyst using a Co(II)-porphyrin-based covalent organic framework (COF) has been reported by Lin *et al*.[15a] The COF powders were deposited on porous, conductive carbon fabric and exhibited a high selectivity for CO formation (90%) with normalized turnover

frequency (TOF) of 0.62 s^{-1} at 550 mV overpotential (compared to an equilibrium potential of 0.11 V vs. RHE[4] as reported for all following overpotentials). In other work, Hu *et al*. have described an efficient method for the synthesis of a heterogeneous catalyst based on the π-π interactions between cobalt(II)-tetraphenylporphyrin (CoTPP) and single wall carbon nanotube (SWCNT), resulting in a catalyst that shows highly selective conversion of CO_2 into CO with 90% faradaic efficiency and a TOF of 0.08 s^{-1} at an overpotential of ~550mV.[15d] In addition, Zhang *et al*. have reported a similar approach with cobalt(II) phthalocyanine/CNT that exhibits highly enhanced electrochemical CO_2 reduction to CO with 95% faradaic efficiency (TOF 4.1 s^{-1}) at 520 mV overpotential.[15e]

Iron-based heterogeneous catalysts have been extensively investigated with Maurin *et al*. reporting iron(III)-porphyrin immobilization onto carbon nanotubes by both π-π stacking and covalent attachment, resulting in 93% CO production (TOF 0.04 s^{-1}) at an overpotential of 480 mV.[15b] In addition, Tatin and coworkers utilized the electrostatic complex formed between a tetracationic iron(III)-porphyrin (WSCAT) and the anionic polymer Nafion adsorbed on carbon powder to create a heterogeneous catalyst on carbon felt. Electrolysis of this composite catalyst resulted in stable catalytic activity over 30 h with a high CO faradaic efficiency of 92% (TOF 0.01 s^{-1}) at an overpotential of 410 mV.[15c] It is notable that the TOFs of the Fe-based metal complexes are significantly lower than those of most cobalt-based molecular catalysts, which may be attributed to the lower energy barrier (less negative potential) for the formation of the catalytic active Co(I) species compared to the reduction of Fe(III) to Fe(0) in the heterogeneous metal complex catalyst systems.

Wang et al. have reported the first example of a Zn(II)-based porphyrin electrocatalyst for electrochemical CO_2 reduction.[16] The heterogenized Zn(II) porphyrin on carbon fiber paper exhibited highly selective CO_2 reduction to CO at moderate overpotential. Unlike other

porphyrin catalysts, interestingly, the Zn(II) porphyrin did not have any redox reactivity at the metal center but rather showed ligand-based CO_2 reduction catalysis.

Although the majority of metal complexes have demonstrated improved catalytic performance through immobilization, most of the catalysts for the production of CO operate at high overpotentials and show poor catalytic durability of less than 5 h, resulting in a low energy efficiency for the electrochemical CO_2 reduction catalysis. Therefore, the goal of a stable, efficient earth-abundant metal complex-based heterogeneous catalyst for the electrocatalytic reduction of CO_2 at low overpotentials has yet to be fully realized.

Herein, we report a simple and facile self-assembly method for the fabrication of reduced graphene oxide frameworks (FePGFs) directly interconnected with 5,10,15,20-tetrakis(4-trimethylammoniumphenyl)porphyrinato iron(III) pentachloride by π-π stacking and electrostatic interactions as an electrocatalyst for CO_2 reduction (**Figure 1**). As a heterogeneous electrocatalyst for the reduction of CO_2 to CO, the as-prepared FePGFs possess a number of advantages including (1) facile and rapid electron transfer, (2) easy electrolyte and CO_2 accessibility, (3) structural robustness, (4) excellent efficiency at low overpotential, and (5) superior long-term stability under the electrochemical reduction conditions.

In contrast to previous work, FePGF modified on glassy carbon plate exhibited excellent electrocatalytic CO_2 reduction performance and stability affording a current density of 0.20 mA cm^{-2} with 97.0% faradaic efficiency for CO production at an overpotential of 480 mV over 24 h, corresponding to a TOF of 0.8 s^{-1} and turnover number (TON) of 69,120. In addition, enhanced catalytic performance is demonstrated using a high surface area carbon fiber paper substrate for the FePGF catalyst in 0.1 M $KHCO_3$ electrolyte. Over a 10 h electrolysis, this results in a higher current density of 1.68 mA cm^{-2} with a 98.7 % CO faradaic efficiency at an overpotential of 430 mV, corresponding to a TOF of 2.9 s^{-1} and 104,400 TON.

2. Results and Discussion

2.1. Fabrication of FePGFs.

The fabrication of FePGFs is summarized in Figure 1. Initially, liquid crystalline graphene oxide (LCGO), synthesized by a modified Hummer's method, was chemically reduced using ascorbic acid at 90°C for 1 h. Subsequently, various amounts of reduced LCGO (*r*LCGO, 1.4, 2.8 and 5.6 mg) were simply mixed with the porphyrin FeTMAP (2 mg dissolved in 30 mL H_2O), in which they spontaneously started to make frameworks presumably by electrostatic interactions between the positively charged functionalities of the FeTMAP and negatively charged *r*LCGO. As *r*LCGO was added into FeTMAP solution, the frameworks formed rapidly and agglomerated in the solution while the residual solution became colourless, indicative of the formation of larger and heavier agglomerates. As indicated in the photographs of the reactions (Figure 1), 5.6 mg of *r*LCGO was the minimum amount of graphene required to visibly consume the 2 mg of FeTMAP. The FePGF electrode was then prepared by drop casting the FePGF dispersion (100 μL) on each side of a glassy carbon plate to give a porphyrin loading of 40 μg cm^{-2} as described in the Experimental section in the Supporting Information. The leaching of catalyst from the FePGF was tested by immersing a FePGF-modified electrode into 20 mL water for 20 h and the amount of porphyrin dissolved from the catalytic film quantified by UV-Vis spectroscopy. As shown in Figure S1 (Supporting Information), less than 0.5 % of the total amount of iron porphyrin leached from the FePGF electrode.

In order to ascertain how much of the FeTMAP was electrochemically active in the FePGFs, the electroactive amounts of FeTMAP on the surface of the modified electrode were estimated based on the plot of peak current of the Fe^{III}/Fe^{II} redox wave as a function of scan rate,[15b, 15c] which showed a linear relationship (Figure S2, Supporting Information). The amount of electroactive FeTMAP on the FePGF-covered surface electrode is calculated according to equation (2),

$$\Gamma = Q/nFA \qquad (2)$$

where Γ is the electroactive amounts of FeTMAP on the modified electrode, Q is the integration of the redox peaks, n is the number of electron consumed, F is the Faraday constant, and A is the electrode area, and is found to be 1.3×10^{-9} mol cm^{-2}. The number of active FeTMAP molecules on the framework surface is 1.6×10^{15} while the number of added FeTMAP molecules in the electrode sample is 4.5×10^{16} corresponding to 3.5% electroactive FeTMAP in the FePGF (see Note S1 in the Supporting Information). While this is surprisingly small, it is similar to that previously observed for the CO_2 reduction activity of Co porphyrins in covalent organic frameworks.[15a]

2.2. Material characterization of FePGF.

Morphological characterization of the FePGFs was carried out with high-resolution transmission electron microscopy (HRTEM) as shown in **Figure 2**. A comparison of the bright field and dark field TEM images of *r*LCGO (Figure 2a,b and a',b', respectively) and FePGF (Figure 2c,d and c',d', respectively) reveals that the FePGF is composed of overlaid large and flat graphene sheets in contrast to *r*LCGO that appears to have a more crumpled sheet structure. It is clear from these images that the FeTMAP has had a significant impact on the morphology of the *r*LCGO, appearing to create a flat, stacked layer-by-layer FePGF structure. Additionally, the distribution of FeTMAP in the FePGF is confirmed by the energy dispersive X-ray spectroscopy (EDS) maps (Figure 2e) and spectra (Figure S3, Supporting Information), which show that N and Fe are homogeneously distributed over the graphene/porphyrin framework composite layer.

The structural and functional integrity of the graphene-bound FeTMAP was investigated by UV-Visible, fluorescence, and Raman spectroscopy. The absorption spectra of LCGO, *r*LCGO, FeTMAP, and FePGF were all obtained from aqueous solutions. As shown in **Figure 3**a, LCGO shows a characteristic absorption peak at 228 nm ($\pi - \pi^*$ transition of aromatic C=C bonds) with a shoulder at around 303 nm ($n - \pi^*$ transition of C=O bonds).[17] After reduction by ascorbic acid at 90 °C for 1h, the absorption peak at 228 nm is red shifted to 260 nm with no 303 nm peak present, inferring that the LCGO was successfully reduced to *r*LCGO by ascorbic acid.[18] The spectrum of FeTMAP exhibits a strong absorption peak at 412 nm, corresponding to the characteristic porphyrin Soret band with weaker Q bands between 500 nm and 700 nm.[19] After formation of FePGF, the Soret band of FeTMAP is red-shifted from 412 nm to 424 nm. This 12 nm shift is half of that reported by Xu *et al*. for the binding of free base TMAP to *r*GO, who demonstrated the molecular flattening of cationic tetraarylporphyrins on graphene due to both π-π stacking and electrostatic interactions between residual negatively charged carboxylate groups on the *r*GO and the cationic groups on the porphyrin.[20] The smaller shift suggests a weaker π-π interaction between the FeTMAP and the *r*LCGO, which is expected due to the presence of the coordinated iron.[21]

The fluorescence spectra of FeTMAP and FePGF were obtained in order to probe the interaction between the excited-state FeTMAP and *r*LCGO (Figure 3c). Upon excitation of FeTMAP at Soret band of 412 nm, strong fluorescence emission peaks centered at 640 nm and 700 nm were recorded. The emission spectrum of the FePGF excited at 424 nm shows no detectable fluorescence emission from FeTMAP, indicative of quenching of the porphyrin excited singlet state by the interacted *r*LCGO sheets as has previously been observed by Xu *et al*.[20a]

The interactions between *r*LCGO and FeTMAP in FePGF were also confirmed by Raman spectroscopy. As shown in Figure 3d, the Raman spectra of both LCGO and *r*LCGO exhibit

two bands at 1331 cm^{-1} and 1585 cm^{-1}, typical of the D and G bands in *r*LCGO.[22] The change in the ratio of the intensities of the two bands (I_D/I_G) show that LCGO (I_D/I_G=1.12) was successfully reduced to *r*LCGO (I_D/I_G=1.24) and the evolution of the more intense and less broad 2D band around 2620 cm^{-1} also indicates better graphitization by chemical reduction of LCGO.[22-23] In contrast, the FePGF I_D/I_G of 1.24 indicates that the incorporated FeTMAP does not affect the aromaticity of the *r*LCGO. However, there is a small shift of the G band from 1585 cm^{-1} (*r*LCGO) to 1594 cm^{-1} indicative of electron doping between *r*LCGO and FeTMAP as a result of the π-π stacking and electrostatic interactions.[24]

In order to gain a deeper insight into the interactions in FePGF, the photoelectron spectroscopy (XPS) analysis for each of FeTMAP, LCGO, rLCGO and FePGF were carried out and the survey and high-resolution spectra for C 1s, N 1s and Fe 2p are shown in Figure S4, **Figure 4** and Figure S5, respectively. The C 1s spectra of LCGO before and after the reduction with ascorbic acid at 90ºC for 1 h are shown in Figure 4a and b. As in previous work,[25] four characteristic C 1s peaks, corresponding to C=C/C-C, C-OH/C-O-C, C=O and O-C=O were observed at 284.5, 286.4, 287.8, and 289.0 eV, respectively. Although the C-O functionalities observed at 286.4 eV were notably decreased after reduction with ascorbic acid, a significant number of C-O groups still remained on the *r*LCGO, indicating that the LCGO was not fully reduced. Furthermore, the atomic percentages of each C 1s peak are shown in Table S1 in the Supporting Information wherein the atomic percentages of the C-O (38.7%) observed in the *r*LCGO are lower than that of LCGO (45.4%), supportive of the mild reduction of LCGO. The C 1s spectrum of FePGF (Figure 4c) showed a much higher intensity C=C/C-C band at 284.5 eV, while the remaining C 1s peaks were little changed compared to that of *r*LCGO. This intensity increase is expected following the binding of the FeTMAP to the *r*LCGO although some intensity increase might also be expected for the band at 286.4 eV due to an increased C-N contribution. Indeed, a comparison of the peak height ratios of the bands

at 286.4 and 287.8 eV show an increase from 5:1 to 6:1. In addition, the N 1s spectrum of FePGF was deconvoluted into three peaks at 398.6, 399.7 and 402.4 eV (Figure 4f). The band at 402.4 eV is due to the cationic N of the $–N^{+}(CH_3)_3$ functional groups on the FeTMAPin FePGF and varies little from that of the pure FeTMAP (Figure S5a).[26] In contrast, the peaks at 398.6 eV (iminic) and 399.7 eV (aminic), assigned to the inner core nitrogens of the porphyrin structure, are at slightly higher binding energy compared to those of FeTMAP.[15b, 27] This is similar to that reported by He *et al.* for a Fe phthalocyanine-graphene complex who postulate that these binding energy shifts are due to charge transfer between the phthalocyanine and the nanocarbon.[28]

Moreover, as shown in Figure 4g-i, Fe2p peaks can only be observed in the FePGF spectrum with peaks at 710.7 and 724.1 eV corresponding to Fe $2p_{3/2}$ and Fe $2p_{1/2}$. These Fe^{III} peaks correlate well to the peaks observed for FeTMAP itself (Figure S5b, 710.6 and 723.3 eV) and other reported Fe porphyrin peaks,[27, 29] indicating that the valence state of the Fe^{III} was not significantly influenced in the formation of FePGF..

2.3. Electrochemical behavior of FeTMAP and FePGF catalysts.

The electrochemical behaviour of FeTMAP as a homogeneous CO_2 reduction catalyst and FePGF as a heterogeneous catalyst was initially investigated by cyclic voltammetry under an atmosphere of Ar or CO_2 as shown in **Figure 5**a. FeTMAP (0.5 mM in 0.1 M KCl, pH 7.1) displayed very similar CV profiles under both Ar and CO_2 to those reported previously.[9a] Under an atmosphere of CO_2, the reduction current density increased at lower negative potentials compared to the CV under Ar, indicative of electrochemical CO_2 reduction. In order to clearly observe the FeTMAP reduction peaks from Fe^{III} to Fe^{0}, Fourier transform AC cyclic voltammetry (FTACV) was performed in Ar saturated 0.1 M KCl electrolyte (pH 7.1) to

minimize the capacitive current in the measurement (frequency: 9 Hz, amplitude: 80 mV and scan rate: 60 mV s^{-1}).[30] As shown in the Figure S6a (Supporting Information), for the FeTMAP homogeneous catalyst, each reduction peak from $Fe^{III/II} \rightarrow Fe^{II/I} \rightarrow Fe^{I/0}$ was clearly observed at 0.19, -0.41, and -0.80 V vs. RHE (hereafter all potentials are reported with respect to RHE).

In contrast, large capacitive currents were observed in the CVs of FePGF, similar to those reported for a MoS_x-*r*GO composite catalyst.[31] While the redox peaks of FeTMAP were not distinct, there appeared to be an apparent decrease in onset potential of reduction under CO_2 compared to Ar. The CV observed in an atmosphere of Ar showed a rapidly increasing current density from -0.72 V, likely due to the hydrogen evolution reaction (HER), whilst the current density measured under CO_2 that may be utilized for either CO production and/or HER, started increasing from -0.56 V, ~200 mV lower. Notably, a relatively small current density was observed in an atmosphere of CO_2 compared to that obtained in Ar, as has been previously observed and ascribed to CO_2 occupying active sites with a slower reaction and thereby impeding HER.[4, 31] The FTACV reveals the Fe reduction peaks for $Fe^{III/II}$, $Fe^{II/I}$ and $Fe^{I/0}$ at 0.13, -0.29, and -0.58 V, respectively (Figure S6b, Supporting Information). Interestingly, the potential required for the reduction of Fe^{I} to Fe^{0}, which directly influences the onset potential of CO_2 reduction, was shifted from -0.80 V to -0.58 V (Inset in Figure 5) following the interaction of the FeTMAP with *r*LCGO, presumably resulting from the delocalized electron density from the π-π stacking. This results in a positive shift (~ 200 mV) in the reduction potential for the generation of the catalytically active species (Fe^{0}). However, these CVs could not provide conclusive evidence about the nature of the reduction process taking place.

2.4. CO_2 reduction activity measurements.

Potentiostatic electrolysis and gas analysis was undertaken to determine the reduction processes. As shown in **Figure 6**a, the onset potentials and faradaic efficiencies were obtained

by gas chromatography (GC) analysis of the gas products at different applied potentials. Experiments were carried out at pH 4.2 in a CO_2 atmosphere using FeTMAP as a homogeneous catalyst (Figure 6a top) and a FePGF modified electrode as the heterogeneous catalyst (Figure 6a bottom) in a 0.1 M KCl electrolyte.

On the basis of the electrolysis results as a function of several potentials, the onset potentials initially generating carbon monoxide (CO) could be estimated. In the case of the FeTMAP homogeneous catalysis, CO was initially produced with 16.6% faradaic efficiency (FE) at -0.59 V, corresponding to 480 mV overpotential for the generation of CO (E^0 for CO_2/CO is 0.11 V in H_2O). The onset potential for FePGF catalysis, on the other hand, was estimated at -0.49 V with an even higher CO generation efficiency of 42.1%. This corresponded to a decrease of the overpotential from 480 mV to 380 mV, attributed to the increased ease of electron transfer to FeTMAP as a result of its interaction with graphene.

As is evident in Figure 6a, 100 % FE of the H_2 and CO generation is not achieved until -0.84 V and -0.54 V for homogeneous and heterogeneous catalysis, respectively. At lower potentials, less than 100 % of the charge is consumed in gas generation although no other products were detected. While only 3.5 % of the porphyrin on the electrode is electrochemically active (*vide supra*), it is likely that residual underlying Fe(III) porphyrin is reduced, which could account for the low FEs.

As can be seen in the electrocatalytic CO_2 reduction results, FePGF showed not only an improved onset potential for CO_2 reduction but also significantly enhanced CO production at lower overpotentials. In the homogeneous catalysis (FeTMAP), the highest conversion of CO_2 into CO was obtained with a faradaic efficiency of 94.5% at an overpotential of 730 mV, while the deposited electrocatalyst (FePGF) afforded the highest CO faradaic efficiency (97.3%) at a significantly lower overpotential (480 mV).

In order to examine the long-term stability of both catalysts, bulk electrolysis was carried out at -0.84 V (FeTMAP) and -0.59 V (FePGF), potentials that produce the highest faradaic efficiencies. During FeTMAP homogeneous catalysis over 10 h (Figure 6b), the average current density was 0.87 mA cm^{-2}, attributed to the high amount of FeTMAP dissolved in the electrolyte (4.7 μmol). During the initial 1 h electrolysis a 94.5 % faradaic efficiency for CO was obtained, but this steadily decreased to 73% CO faradaic efficiency after 10 h, which may be attributed to the deactivation of FeTMAP by aggregation, porphyrin reduction and/or demetallation, degradation processes that have been proposed for metallo- porphyrins and phthalocyanine electrocatalysts.[32] Based on these results, the FeTMAP TOF and turnover number (TON) were calculated as 0.003 s^{-1} and 108, respectively.

In comparison, bulk electrolysis with FePGF at -0.59 V (corresponding to 480 mV overpotential) showed significantly stable catalytic activity that maintained a very high CO selectivity of 93% faradaic efficiency after 24 h (see entry 2, Table 1). While the average current density of 0.20 mA cm^{-2} was lower than for homogeneous catalysis reflecting the reduced amount of graphene-bound porphyrin available at the electrode, CO was consistently generated with an average of 97.0% faradaic efficiency. Furthermore, the FePGF catalyst TOF (0.8 s^{-1}) and TON (69,120) were vastly improved (see Note S2 in the Supporting Information for details). Comparing the FePGF heterogeneous catalyst to other reported metal complex immobilized catalysts for electrochemical CO_2 reduction (Table 1) shows that not only does it exhibit one of the lowest potentials at maximum faradaic efficiency for CO generation (see column 2, Table 1) but it also has one of the highest TOFs at similar potentials to those reported in other papers (Figure S7, Supporting Information), making FePGF one of the most promising and stable catalysts reported.

In order to assess the integrity of the FeTMAP in the FePGF following the extended 24 h bulk electrolysis, the FePGF was recovered from the electrode by sonication in water, and the

resulting suspension examined by UV-Vis and fluorescence spectroscopy, with TEM images obtained from the recovered powder. As shown in Figure S8 and S9 (Supporting Information), a clear absorption peak at 424 nm was still evident in the UV-Vis spectrum and emission peaks were not observed at 640 nm and 700 nm, indicating that FeTMAP was still bound to the graphene layer after the extended electrolysis. As can be seen in the Fe 2p XPS spectrum (Figure S10, Supporting Information), moreover, it is found that the Fe^{III} valence state was well maintained during 24 h electrolysis.

2.5. pH dependence.

In order to assess the effect of pH on the CO_2 reduction, the pH of 0.1 M KCl electrolyte was adjusted to pH 6.8 under 1 atm CO_2. As revealed in the gas evolution measurements (CO or H_2 production) at various applied potentials at neutral pH (Figure S11a, Supporting Information), FePGF showed high selectivity for electrochemical CO_2 conversion into CO over a wide potential range, resulting in the highest faradaic efficiency of 95% for CO at a potential of -0.54 V, lower than for pH 4.2 and corresponding to a smaller 430 mV overpotential, with the onset potential shifted from -0.49 V to -0.39V. Furthermore, the faradaic efficiency reached 100% at a lower potential (-0.44 V at pH 6.8 vs -0.54 V at pH 4.2), which we attribute to the differences in proton sources utilized for proton coupled electron transfer reaction for the reduction at different pHs.[33] Moreover, the HER resulting from the reduction of carbonic acid (H_2CO_3) and/or hydrated protons may be relatively suppressed in a neutral electrolyte, resulting in improved selectivity of CO production.[9a]

In the long-term performance measurement of CO_2 reduction at neutral pH (Figure S11b, Supporting Information), stable catalytic activity was again observed over 10 h, resulting in an average 94.2% CO generation with stable current density at 0.27 mA cm^{-2}, and TOF and TON of 1.0 s^{-1} and 36,000, respectively (Table 1).

2.6. Energy efficiency calculation.

Energy efficiency (EE) is the most critical parameter to determine overall energy utilization in the cathodic and anodic reactions. The cathodic half reaction EEs were calculated with an assumed anode overpotential (for water oxidation) of at least 400 mV; this is an important part of the energy cost of the generation of the gas products at the cathode. EE is determined by the following equation (3),[34]

$$\mathrm{EE}\ (\%) = \Delta E^0 / \Delta E^{\mathrm{Applied}} \times \mathrm{FE} \qquad (3)$$

where ΔE^0 is the equilibrium full cell potential ($E^0_{CO_2/CO} - E^0_{\text{Water oxidation}} = -0.11\ \mathrm{V} - 1.23\ \mathrm{V} = -1.34\ \mathrm{V}$), $\Delta E^{\mathrm{Applied}}$ is the applied full cell potential ($E^{\mathrm{Applied}}_{CO_2/CO} - E^{\mathrm{Assumed}}_{\text{Water oxidation}} = -0.59\ \mathrm{V} - 1.63\ \mathrm{V} = -2.22\ \mathrm{V}$), and FE is the average faradaic efficiency for CO (97.0 %) at -0.59 V for the 24 h electrolysis in 0.1 M KCl electrolyte (pH 4.2).

From this calculation, an EE of 58.5% was obtained for the catalytic reaction of FePGF, the highest reported for metal complex immobilized catalysts (see Table 1, for a comparison with other reported catalytic systems), highlighting its promise as an energy-efficient catalyst for the production of CO from CO_2.

2.7. Possible CO_2 reduction mechanism of the FePGF catalyst.

Comparing the TOF and TON values of the homogeneous FeTMAP and heterogeneous FePGF catalytic systems, it is clear that a dramatic enhancement in catalytic activities for CO_2 reduction was achieved when the catalytically active species, FeTMAP, was well interconnected with the graphene layers forming frameworks. As mentioned above, delocalization of electron density on the FeTMAP molecule interacting with *r*LCGO by π-π

stacking may be one of the critical reasons for the shift in two of the three reduction potentials of FeTMAP in FePGF toward more positive potential. In order to gain some mechanistic insight into this enhanced reactivity, a Tafel analysis was undertaken (Figure S12, Supporting Information).

Based on previous studies,[35] CO generation proceeds by a two-electron two-proton reduction with the initial electron transferred onto CO_2 to form an adsorbed $CO_2^{\bullet-}$ intermediate on the surface of the catalyst with less negative potentials required to effect the following proton-assisted reduction steps. Forming the adsorbed $CO_2^{\bullet-}$ intermediate is considered the rate determining step. As shown in Figure S12 (Supporting Information), the Tafel slopes for homogeneous FeTMAP and heterogeneous FePGF catalysis were 129 and 96 mV dec^{-1}, respectively, which are comparable to the theoretical value of 118 mV dec^{-1} for the initial single electron injection to form the $CO_2^{\bullet-}$ intermediate.[35c] However, the improved Tafel value of 96 mV dec^{-1} obtained for the FePGF heterogeneous catalysis may be due to improved electron-transfer kinetics resulting from enhanced electron transfer through the well-constructed graphene framework. In addition, it may imply that the heterogeneous electrokinetics of CO_2 conversion into CO is not dominantly determined by initial single electron transfer; stabilisation of the $CO_2^{\bullet-}$ intermediate on the graphene-bonded Fe^0TMAP may be capable of reducing the energy barrier for electrochemical CO_2 reduction.

Enhanced electrochemical CO_2 reduction has also been observed using binuclear metalloenzymes (i.e. binuclear Ni and Fe centers in carbon monoxide dehydrogenase (CODH)[36] and a cofacial Fe porphyrin dimer[37]), in which the activation of CO_2 between metal centers separated at suitable distances (less than 6.2 Å) occurs affording the enhanced reduction. Thus, if Fe porphyrins existed face-to-face in FePGF, ideally separated by 3.4–4.0 Å, this would provide sufficient space to bind the linear CO_2 molecules (2.32 Å) and contribute

to the push-pull activation of the CO_2 molecule,[37a] a similar reduction enhancement might be expected.

2.8. State-of-the-art.

The performance of the FePGF heterogeneous catalyst was compared with other reported metal complex heterogeneous catalysts using similar experimental conditions such as the use of a high surface area electrode substrate and the commonly used bicarbonate-based electrolyte. A FePGF catalytic film was deposited on a high surface area carbon fiber paper (CFP, 1 cm^{-2} geometric surface area) and bulk electrolysis was carried out at -0.54 V (FePGF) for 10 h in 0.1M $KHCO_3$ under a CO_2 atmosphere (pH 6.8) as described in the Supporting Information. Prior to electrolysis, the amount of electrochemically active porphyrin was estimated using CV at different scan rates (Figure S13, Supporting Information). The FePGF/CFP exhibited a slightly higher amount of electrochemically active porphyrin (3.0×10^{-9} mol cm^{-2}) compared to that on the glassy carbon electrode, presumably due to the higher surface area of the CFP.

As shown in the CV profile of FePGF/CFP under a CO_2 atmosphere (**Figure 7**a), FePGF/CFP produced ~22.6 mA cm^{-2} at -0.98 V, which is more than a five-fold increase in current density compared to that obained on glassy carbon in a 0.1M KCl electrolyte (Figure 5b). For the electrolysis at -0.54 V, the FePGF/CFP showed current density as high as 1.68 mA cm^{-2} with ~ 98.7% of the electrons utilized for CO generation over a 10 h electrolysis (Figure 7b). On the basis of the electrolysis results, the TOF and TON for CO production of FePGF/CFP was found to be 2.9 s^{-1} and 104,400, respectively.

In particular, the current density of 1.68 mA cm^{-2} generated by the FePGF catalysis can be considered the highest of all the immobilized metalloporphyrin heterogeneous catalysts (Table 1) if the active number of molecules in each catalytic system is considered. Compared to the other immobilized metalloporphyrin heterogeneous catalysts (entry 4, 5, 6, 9, 12, Table 1), FePGF has one of the smallest amounts of active species in the catalyst with the second highest

current density; the CoTPP/SWNT catalyst (entry 9, Table 1) has twice the current density but almost 100 times the active catalyst. Compared to the WSCAT/Nafion/Carbon powder catalyst (entry 4) in which the same porphyrin (FeTMAP) was utilized to form the heterogeneous catalyst, the FePGF catalyst exhibited significantly higher catalytic activity, particularly in TOF (2.9 s^{-1} FePGF at -0.54 V vs. 0.01 s^{-1} WSCAT/Nafion/Carbon powder at -0.52 V). This may be due to the well-organized framework structure between porphyrin and *r*LCGO without reduced aggregation of the porphyrin molecules in the FePGF.

In contrast, while the reported metallophthalocyanine heterogeneous catalysts (Table 1, entries 7, 8, 10 and 11) all show higher current densities, with the CoPc/MWCNT catalyst (entries 7,8) exhibiting an order of magnitude higher current density, these catalysts typically have 2-6 times the amount of active catalyst than for the FePGF. In addition, all the metallophthalocyanine catalysts show lower TON values highlighting the catalytic durability of the FePGF catalyst.

Overall, it appears that the direct binding of the Fe porphyrin to a carbon substrate *via* electrostatic or π-π stacking significantly improves electron transfer between the iron catalyst and the conductive carbon affording a catalyst with one of the highest CO_2 conversion efficiencies (98.7%) at one of the lowest potentials (-0.54 V corresponding to 430 mV overpotential) of the reported heterogeneous metal complex catalyst systems.

2.9. LCGO vs. reduced LCGO.

The preparation of the FePGF required at least partial reduction of the LCGO as described above. Nonetheless, it was not clear how reduced the graphene needed to be to create an effective catalyst. LCGO itself has the potential to create more electrostatic interactions with the cationic porphyrin compared to a mildly reduced LCGO (*r*LCGO), whilst a more highly reduced LCGO (*hr*LCGO) could provide less electrostatic interactions but more π-π

interactions and high conductivity for electron-transfer to the porphyrin catalyst (**Figure 8a**). Consequently, two more porphyrin-based graphene composite catalysts were prepared and their electrochemical catalytic activity explored.

For this study, an LCGO-FeTMAP composite was prepared as described in the Supporting Information and deposited on CFP. To investigate CO_2 reduction, analysis of the gas produced by LCGO-FeTMAP was carried out during electrolysis at -0.54 V in 0.1M $KHCO_3$. As shown in Figure 8b, the current density from LCGO-FeTMAP showed a significant drop over the first 250 s while there was no detection of gas products in the first 120 s of electrolysis time (Figure 8c). This suggested that, at least initially (120 s), all current was utilized for the electrochemical reduction of LCGO to *r*LCGO until sufficient reduction had occurred to allow H2/CO catalytic production to take place. After 1 h electrolysis, however, the LCGO-FeTMAP composite showed very similar CO_2 reduction performance (99.3% CO FE and 0.5% H_2 FE) to that obtained by FePGF likely due to the LCGO-FeTMAP catalyst reaching the same level of reduction as the FePGF; it is worthy of note that the FePGF catalyst itself was always subject to a CV preconditioning (see Electrochemical Measurements, Supporting Information). However, the LCGO-FeTMAP catalyst exhibited a lower current density of 1.6 mA cm^{-2} than that FePGF (2.2 mA cm^{-2}) after 3600 s that may be a result of the loss of porphyrin catalyst during reduction.

To investigate the importance of the degree of graphene reduction on the electrochemical CO_2 reduction performance, a more severe chemical reduction of LCGO with ascorbic acid at 90℃ for 12 h was undertaken. The resulting *hr*LCGO was then utilized for the formation of an *hr*LCGO-FeTMAP composite (see the Supporting Information for details). The *hr*LCGO-FeTMAP catalyst was coated on CFP and electrolysis was performed at -0.54 V. As shown in Figure 8b, the catalyst showed much lower current density (0.32 mA cm^{-2}) at 3600 s, which may have been a result of a reduced amount of electrochemically active porphyrin due to fewer

functionalities on the *hr*LCGO. Moreover, slightly lower catalytic activity for CO production (86.7% FE) was observed with ~14.3% H_2 conversion (Figure 8c). This may be due to the relatively small number of iron porphyrin CO_2 catalytic active sites compared to the proton reduction sites on *hr*LCGO. Attempts to measure the amount of electrochemically active porphyrin on this electrode were made given this evidence for a reduced amount, but were not successful due to the poor CV response from the porphyrin. Interestingly, the CO selectivity of *hr*LCGO-FeTMAP gradually decreased with electrolysis time and afforded 51.2% CO FE and 48.5% H_2 FE after 10 h electrolysis (Figure S14, Supporting Information), which may be related to the decreased stability of the more reduced framework. Therefore, it appears that a framework-based structure such as the FePGF, that has a balance of electrostatic groups and aromatic areas for π-π interactions, could be critical for the long-term catalytic performance of a FeTMAP heterogeneous catalyst on graphene.

3. Conclusion

In conclusion, we have synthesized porphyrin/graphene frameworks (FePGF) composed of a tetracationic Fe(III)-porphyrin and partially reduced LCGO (*r*LCGO) by utilizing the electrostatic interactions between the ammonium cations of the Fe porphyrin and the carboxylate anions of the *r*LCGO, affording a facile and simple self-assembly method. This new type of heterogeneous framework-based catalyst has been investigated on glassy carbon for electrochemical CO_2 reduction to CO in water at both acidic (pH 4.2) and neutral (pH 6.8) pHs. FePGF exhibited an average faradaic efficiency for CO production of 97.0% at -0.59 V (corresponding to 480 mV overpotential for CO generation) with negligible H_2 generation over 24 h, corresponding to a TOF of 0.8 s^{-1} and 58.5% energy efficiency. In addition, the catalytic activity of FePGF deposited on a carbon fiber paper was examined to compare with previously reported heterogeneous metal complex catalysts. This higher surface area electrocatalyst exhibited significantly enhanced CO_2 reduction to CO with 98.7% CO faradaic efficiency at

an overpotential as low as 430 mV for 10 h, corresponding to a TOF of 2.9 s^{-1} and 104,400 TON. Consequently, FePGF outperforms current state-of-the-art immobilized metal complex electrocatalysts for the conversion of CO_2 into CO.

To examine the effect of the degree of LCGO reduction, two more composites of the cationic porphyrin FeTMAP and LCGO itself as well as a highly reduced LCGO were prepared and their catalytic activity on carbon fiber paper compared to that of FePGF. For the LCGO-FeTMAP catalyst electrolysis, it was apparent that an initial reduction of the LCGO occurred prior to CO_2 catalysis. Nonetheless, after 1 h electrolysis, the CO production reached a similar level to that of the FePGF albeit with a lower current density. In contrast, the more reduced *hr*LCGO-FeTMAP catalyst showed a small drop in CO selectivity but a large change in current density after 1 h electrolysis. In addition, the stability of the *hr*LCGO-FeTMAP catalyst was significantly reduced after 10 h with an accompanying large drop in CO selectivity. Thus, the heterogeneous framework catalyst FePGF appears to offer the required balance of electrostatic interaction and reduced character affording both high catalytic efficiency and long term stability.

The excellent performance of FePGF may be explained by several factors. The formation of the graphene framework likely not only enhances electron transfer but also delocalizes the electron density on the FeTMAP, enabling a positive shift in the Fe^{I}TMAP to Fe^{0}TMAP reduction potential. Cofacial Fe porphyrins within the framework may allow the stabilization of CO_2 by a push-pull mechanism in between the Fe centers. The highly porous framework-based structure formed by the layered graphene appears to not only promote the contact area between FeTMAP and electrolytes, facilitating CO_2 access, but also maintain stable catalysis with consistent faradaic efficiency for CO formation during 24 h electrolysis. A more in-depth

study of these factors is currently being undertaken in order to better understand the catalytic activity of this porphyrin-graphene composite.

The catalytic potential of this porphyrin/graphene framework concept could be further enhanced using three dimensional hierarchical structures such as sponges and fibers. Varying the porphyrin metal or even the molecular catalyst itself could also lead to the conversion of CO_2 into a variety of other value-added chemicals and such studies are underway.

4. Experimental Section

Synthesis of FePGFs: The porphyrin FeTMAP (2 mg) was dissolved in DI water (30 mL) to make a dilute solution (66.6 μg mL^{-1}). The FeTMAP solution (30 mL) was mixed with a dispersion of *r*LCGO (2 mL, 2.8 mg mL^{-1}) leading to the spontaneous formation of agglomerates. After forming the agglomerated frameworks, unbound FeTMAP was removed following centrifugation by separating the reddish coloured centrifugate from the agglomerates. This process was repeated until the supernatant solution turned colourless. Finally, DI water (5 mL) was added to the resulting agglomerates and then the suspension was vigorously dispersed using a vortex mixer until it was visually well-dispersed.

Synthesis of LCGO-FeTMAP composites: FeTMAP (2 mg) was dissolved in H_2O (30 mL) and mixed with LCGO dispersion (1 mL, 5.6 mg mL^{-1}) following which they spontaneously aggregated as observed in the preparation of FePGF. After forming the agglomerates, unbound FeTMAP was removed following centrifugation by separating the reddish coloured centrifugate from the agglomerates. Finally, H_2O (5 mL) was added to the resulting agglomerates and then the suspension was homogeneously dispersed using a vortex mixer.

Synthesis of hrLCGO-FeTMAP composites: The *hr*LCGO was prepared using ascorbic acid in deionized (DI) water. Specifically, ascorbic acid (16.8 mg) was added to a water dispersed LCGO solution (10 mL, 0.56 mg mL^{-1}) and heated at 90°C for 12 h, during which *r*LCGO

sheets were loosely interconnected as a graphene hydrogel. Upon cooling, the resulting material was sonicated for 3 h to obtain an *hr*LCGO dispersion. The dispersion was centrifuged (11,000 rpm for 10 min) and the supernatant removed. The residual *hr*LCGO was redispersed in DI water (5.6 mL) to give a concentration of 1 mg mL^{-1}.

FeTMAP (2 mg) was dissolved in H_2O (30 mL) and mixed with LCGO dispersion (5.6 mL, 1 mg mL^{-1}) The resulting solution lost much of its colour, indicative of the interaction between the residual carboxylate anions of *hr*LCGO and the cationic groups of the FeTMAP, along with the precipitation of agglomerates. Unbound FeTMAP was removed following centrifugation by separating the reddish coloured centrifugate from the agglomerates. Finally, H_2O (5 mL) was added to the agglomerates and the resulting suspension was homogeneously dispersed using a vortex mixer.

***Electrochemical measurements*:** All of the electrochemical measurements were carried out in an airtight two compartment electrochemical cell purchased from Pine Instruments (USA) with clearly polished glassy carbon plate (surface area of each side: 1 cm^2), platinum wire counter electrode, and Ag/AgCl reference electrode (3.5 M KCl), using a potentiostat (CH Instruments, 650D, USA). FePGF solutions (100 μL) were drop-cast onto each side of the glassy carbon plate to form the FePGF modified electrode, which was dried under a fumehood at room temperature. The as-prepared FePGF electrode was immersed into an Ar-saturated 0.1M KCl electrolyte and cycled from 0 V to -1.6 V (vs. Ag/AgCl (3.5 M KCl)) at a scan rate of 100 mV s^{-1} for 6 cycles in order to precondition the electrode. Following this, cyclic voltammetry (CV) measurements were taken under the same conditions either in a 0.1 M KCl electrolyte under an Ar (pH 7.1) or CO_2 atmosphere (pH 4.2).

For the high surface area CFP electrode development, 100 μL of the catalyst dispersion (LCGO-FeTMAP, FePGF or *hr*LCGO-FeTMAP) were drop-cast onto each side of the CFP

(geometric surface area of 1 cm^{-2}) to form the catalyst-modified electrode, which was dried under a fumehood at room temperature. The as-prepared FePGF and *hr*LCGO-FeTMAP electrodes were immersed into an Ar-saturated 0.1M $KHCO_3$ electrolyte and cycled from 0 V to -1.6 V (vs. Ag/AgCl (3.5 M KCl)) at a scan rate of 100 mV s^{-1} for 6 cycles in order to precondition the electrode. (Preconditioning was not carried out for the LCGO-FeTMAP electrode.) Following this, cyclic voltammetry (CV) measurements were taken under the same conditions either in a 0.1 M $KHCO_3$ electrolyte under an Ar (pH 8.3) or CO_2 atmosphere (pH 6.8).

All potentials in this study were adjusted to the reversible hydrogen electrode (RHE) reference scale using the formula:

$$\mathbf{E\ (vs.\ RHE) = Applied\ potential\ (vs.\ Ag/AgCl) + 0.210\ V + 0.059\ V \times pH}$$

***Gas product analysis*:** Bulk electrolysis was carried out to detect the gas products for CO_2 reduction by gas chromatography (GC, Shimadzu, GC-08) equipped with a 6-foot molecular sieve 5 Å column and a thermal conductivity detector (TCD). The column was kept at 90°C while the detector was at 100°C for the analysis. Gas production was calculated using calibration curves (CO: 6.30×10^{11} area mol^{-1}, H_2: 7.32×10^{12} area mol^{-1}) made by sampling known volumes of CO and H_2 gas.

From the result of the GC analysis, the faradaic efficiency of each experiment was calculated using equation below, where *Q* is the charge passed during the bulk electrolysis, *z* is the number of electrons for CO, *n* is the number of moles of CO based on GC analysis, and *F* is the Faraday constant.

$$\mathbf{Faradaic\ efficiency}\ (\%) = \frac{\mathbf{Q_{Experimental}}}{\mathbf{Q_{Theoretical}}} \times \mathbf{100}$$

$$= \frac{\mathbf{z \times n \times F}}{\mathbf{Q}} \times \mathbf{100}$$

Supporting Information
Supporting Information is available from the Wiley Online Library or from the author.

Acknowledgements
This work was supported by the ARC Centre of Excellence Scheme (Project Number CE 140100012). JC also thanks the University of Wollongong (UOW) for a University Postgraduate Award. DRM is grateful for support from the Australian Research Council for his Australian Laureate Fellowship. The authors thank the Materials Node of the Australian National Fabrication Facility (ANFF) and the UOW Electron Microscopy Centre for their facilities and research support.

Received: ((will be filled in by the editorial staff))
Revised: ((will be filled in by the editorial staff))
Published online: ((will be filled in by the editorial staff))

References

[1] a) W. Tu, Y. Zhou, Z. Zou, *Adv. Mater.* **2014**, *26*, 4607-4626; b) Y. Izumi, *Coord. Chem. Rev.* **2013**, *257*, 171-186; c) M. Mikkelsen, M. Jørgensen, F. C. Krebs, *Energy Environ. Sci.* **2010**, *3*, 43-81; d) H. Takeda, C. Cometto, O. Ishitani, M. Robert, *ACS Catal.* **2016**, *7*, 70-88; e) Q. Lu, F. Jiao, *Nano Energy* **2016**, *29*, 439-456.

[2] a) T. W. Woolerton, S. Sheard, E. Reisner, E. Pierce, S. W. Ragsdale, F. A. Armstrong, *J. Am. Chem. Soc.* **2010**, *132*, 2132-2133; b) W. C. Chueh, C. Falter, M. Abbott, D. Scipio, P. Furler, S. M. Haile, A. Steinfeld, *Science* **2010**, *330*, 1797-1801; c) C. D. Windle, R. N. Perutz, *Coord. Chem. Rev.* **2012**, *256*, 2562-2570; d) T. E. Rosser, C. D. Windle, E. Reisner, *Angew. Chem., Int. Ed.* **2016**, *128*, 7514-7518; e) D. D. Zhu, J. L. Liu, S. Z. Qiao, *Adv. Mater.* **2016**, *28*, 3423-3452.

[3] a) D. T. Whipple, P. J. Kenis, *J. Phys. Chem. Lett.* **2010**, *1*, 3451-3458; b) J. Albo, M. Alvarez-Guerra, P. Castaño, A. Irabien, *Green Chem.* **2015**, *17*, 2304-2324; c) J. Durst, A. Rudnev, A. Dutta, Y. Fu, J. Herranz, V. Kaliginedi, A. Kuzume, A. A. Permyakova, Y. Paratcha, P. Broekmann, *Chimia* **2015**, *69*, 769-776.

[4] Y. Hori, in *Modern Aspects of Electrochemistry, Vol. 42* (Eds.: C. G. Vayenas, R. E. White, M. E. Gamboa-Aldeco), Springer, New York, NY, **2008**, pp. 89-189.

[5] a) M. Liu, Y. Pang, B. Zhang, P. De Luna, O. Voznyy, J. Xu, X. Zheng, C. T. Dinh, F. Fan, C. Cao, *Nature* **2016**, *537*, 382-386; b) D. Gao, H. Zhou, J. Wang, S. Miao, F. Yang, G. Wang, J. Wang, X. Bao, *J. Am. Chem. Soc.* **2015**, *137*, 4288-4291; c) A. Klinkova, P. D. Luna, C.-T. Dinh, O. Voznyy, E. M. Larin, E. Kumacheva, E. H. Sargent, *ACS Catal.* **2016**, *6*, 8115-8120.

[6] a) W. Luc, C. Collins, S. Wang, H. Xin, K. He, Y. Kang, F. Jiao, *J. Am. Chem. Soc.* **2017**, *139*, 1885-1893; b) Y. Zhao, C. Wang, G. G. Wallace, *J. Mater. Chem. A* **2016**, *4*, 10710-10718.

[7] Q. Li, J. Fu, W. Zhu, Z. Chen, B. Shen, L. Wu, Z. Xi, T. Wang, G. Lu, J.-j. Zhu, *J. Am. Chem. Soc.* **2017**, *139*, 4290-4293.

[8] a) M. Asadi, K. Kim, C. Liu, A. V. Addepalli, P. Abbasi, P. Yasaei, P. Phillips, A. Behranginia, J. M. Cerrato, R. Haasch, *Science* **2016**, *353*, 467-470; b) J. Choi, T. M. Benedetti, R. Jalili, A. Walker, G. G. Wallace, D. L. Officer, *Chem. - Eur. J.* **2016**, *22*, 14158-14161.

[9] a) C. Costentin, M. Robert, J.-M. Savéant, A. Tatin, *Proc. Natl. Acad. Sci. U. S. A.* **2015**, *112*, 6882-6886; b) S. Roy, B. Sharma, J. Pecaut, P. Simon, M. Fontecave, P. D. Tran, E. Derat, V. Artero, *J. Am. Chem. Soc.* **2017**, *139*, 3685-3696; c) I. Azcarate, C. Costentin, M. Robert, J.-M. Savéant, *J. Am. Chem. Soc.* **2016**, *138*, 16639-16644.

[10] a) C. Costentin, M. Robert, J.-M. Savéant, *Chem. Soc. Rev.* **2013**, *42*, 2423-2436; b) M. Rakowski Dubois, D. L. Dubois, *Acc. Chem. Res.* **2009**, *42*, 1974-1982.

[11] a) C. Oloman, H. Li, *ChemSusChem* **2008**, *1*, 385-391; b) N. S. Lewis, D. G. Nocera, *Proc. Natl. Acad. Sci. U. S. A.* **2006**, *103*, 15729-15735; c) J. Bonin, A. Maurin, M. Robert, *Coord. Chem. Rev.* **2016**, *334*, 184-198.

[12] Y.-J. Zhang, V. Sethuraman, R. Michalsky, A. A. Peterson, *ACS Catal.* **2014**, *4*, 3742-3748.

[13] G. Balducci, G. Chottard, C. Gueutin, D. Lexa, J.-M. Saveant, *Inorg. Chem.* **1994**, *33*, 1972-1978.

[14] a) C. Costentin, M. Robert, J.-M. Savéant, *Curr. Opin. Elec.* **2017**, *2*, 26-31; b) R. M. Bullock, A. K. Das, A. M. Appel, *Chem. - Eur. J.* **2017**, *23*, 7626-7641.

[15] a) S. Lin, C. S. Diercks, Y.-B. Zhang, N. Kornienko, E. M. Nichols, Y. Zhao, A. R. Paris, D. Kim, P. Yang, O. M. Yaghi, *Science* **2015**, *349*, 1208-1213; b) A. Maurin, M. Robert, *Chem. Commun.* **2016**, *52*, 12084-12087; c) A. Tatin, C. Comminges, B. Kokoh, C. Costentin, M. Robert, J.-M. Savéant, *Proc. Natl. Acad. Sci. U. S. A.* **2016**, *113*, 5526-5529; d) X. M. Hu, M. H. Rønne, S. U. Pedersen, T. Skrydstrup, K. Daasbjerg, *Angew. Chem., Int. Ed.* **2017**, *56*, 6468-6472; e) X. Zhang, Z. Wu, X. Zhang, L. Li, Y. Li, H. Xu, X. Li, X. Yu, Z. Zhang, Y. Liang, *Nat. Commun.* **2017**, *8*, 14675.

[16] Y. Wu, J. Jiang, Z. Weng, M. Wang, D. l. L. Broere, Y. Zhong, G. W. Brudvig, Z. Feng, H. Wang, *ACS Cent. Sci.* **2017**, *3*, 847-852.

[17] D. Li, M. B. Müller, S. Gilje, R. B. Kaner, G. G. Wallace, *Nat. Nanotechnol.* **2008**, *3*, 101-105.

[18] D. C. Marcano, D. V. Kosynkin, J. M. Berlin, A. Sinitskii, Z. Sun, A. Slesarev, L. B. Alemany, W. Lu, J. M. Tour, *ACS Nano* **2010**, *4*, 4806-4814.

[19] A. K. Rahiman, K. S. Bharathi, S. Sreedaran, V. Narayanan, *Catal. Lett.* **2009**, *127*, 175-182.

[20] a) Y. Xu, L. Zhao, H. Bai, W. Hong, C. Li, G. Shi, *J. Am. Chem. Soc.* **2009**, *131*, 13490-13497; b) J. Geng, H.-T. Jung, *J. Phys. Chem. C* **2010**, *114*, 8227-8234.

[21] C. A. Hunter, J. K. Sanders, *J. Am. Chem. Soc.* **1990**, *112*, 5525-5534.

[22] S. H. Aboutalebi, R. Jalili, D. Esrafilzadeh, M. Salari, Z. Gholamvand, S. Aminorroaya Yamini, K. Konstantinov, R. L. Shepherd, J. Chen, S. E. Moulton, *ACS Nano* **2014**, *8*, 2456-2466.

[23] V. C. Tung, M. J. Allen, Y. Yang, R. B. Kaner, *Nat. Nanotechnol.* **2009**, *4*, 25-29.

[24] A. Das, S. Pisana, B. Chakraborty, S. Piscanec, S. Saha, U. Waghmare, K. Novoselov, H. Krishnamurthy, A. Geim, A. Ferrari, *Nat. Nanotechnol.* **2008**, *3*, 210-215.

[25] a) J. Zhang, H. Yang, G. Shen, P. Cheng, J. Zhang, S. Guo, *Chem. Commun.* **2010**, *46*, 1112-1114; b) S. Stankovich, D. A. Dikin, R. D. Piner, K. A. Kohlhaas, A. Kleinhammes, Y. Jia, Y. Wu, S. T. Nguyen, R. S. Ruoff, *Carbon* **2007**, *45*, 1558-1565.

[26] R. K. Blundell, P. Licence, *Phys. Chem. Chem. Phys.* **2014**, *16*, 15278-15288.

[27] M. Wang, W. Zhu, Q. Wang, Y. Yang, H. Zhou, F. Zhang, L. Zhou, J. M. Razal, G. G. Wallace, J. Chen, *Green Energy Environ.* **2017**, *2*, 285-293.

[28] a) L. Cui, Y. Liu, X. He, *J. Electroanal. Chem.* **2014**, *727*, 91-98; b) L. Cui, G. Lv, Z. Dou, X. He, *Electrochim. Acta* **2013**, *106*, 272-278.

[29] A. Maurin, M. Robert, *Chem. Commun.* **2016**, *52*, 12084-12087.

[30] a) A. M. Bond, N. W. Duffy, S.-X. Guo, J. Zhang, D. Elton, *Anal. Chem.* **2005**, *77*, 186A; b) S. O. Engblom, J. C. Myland, K. B. Oldham, *J. Electroanal. Chem.* **2000**, *480*, 120-132; c) D. Gavaghan, A. Bond, *J. Electroanal. Chem.* **2000**, *480*, 133-149.

[31] F. Li, S.-F. Zhao, L. Chen, A. Khan, D. R. MacFarlane, J. Zhang, *Energy Environ. Sci.* **2016**, *9*, 216-223.

[32] a) Z. Weng, Y. Wu, M. Wang, J. Jiang, K. Yang, S. Huo, X.-F. Wang, Q. Ma, G. W. Brudvig, V. S. Batista, *Nat. Commun.* **2018**, *9*, 415; b) I. Hod, M. D. Sampson, P. Deria, C. P. Kubiak, O. K. Farha, J. T. Hupp, *ACS Catal.* **2015**, *5*, 6302-6309.

[33] C. Costentin, S. Drouet, G. Passard, M. Robert, J.-M. Savéant, *J. Am. Chem. Soc.* **2013**, *135*, 9023-9031.

[34] a) J. Medina-Ramos, J. L. DiMeglio, J. Rosenthal, *J. Am. Chem. Soc.* **2014**, *136*, 8361-8367; b) B. Kumar, V. Atla, J. P. Brian, S. Kumari, T. Q. Nguyen, M. Sunkara, J. M. Spurgeon, *Angew. Chem., Int. Ed.* **2017**, *56*, 3645-3649.

[35] a) Q. Lu, J. Rosen, Y. Zhou, G. S. Hutchings, Y. C. Kimmel, J. G. Chen, F. Jiao, *Nat. Commun.* **2014**, *5*, 3242; b) Y. Chen, M. W. Kanan, *J. Am. Chem. Soc.* **2012**, *134*, 1986-1989; c) Y. Chen, C. W. Li, M. W. Kanan, *J. Am. Chem. Soc.* **2012**, *134*, 19969-19972; d) S. Gao, Y. Lin, X. Jiao, Y. Sun, Q. Luo, W. Zhang, D. Li, J. Yang, Y. Xie, *Nature* **2016**, *529*, 68-72.

[36] W. Shin, S. H. Lee, J. W. Shin, S. P. Lee, Y. Kim, *J. Am. Chem. Soc.* **2003**, *125*, 14688-14689.

[37] a) E. A. Mohamed, Z. N. Zahran, Y. Naruta, *Chem. Commun.* **2015**, *51*, 16900-16903; b) Z. N. Zahran, E. A. Mohamed, Y. Naruta, *Sci. Rep.* **2016**, *6*, 24533.

[38] A. Maurin, M. Robert, *J. Am. Chem. Soc.* **2016**, *138*, 2492-2495.

[39] W. Kramer, C. McCrory, *Chem. Sci.* **2016**, *7*, 2506-2515.

[40] N. Morlanés, K. Takanabe, V. Rodionov, *ACS Catal.* **2016**, *6*, 3092-3095.

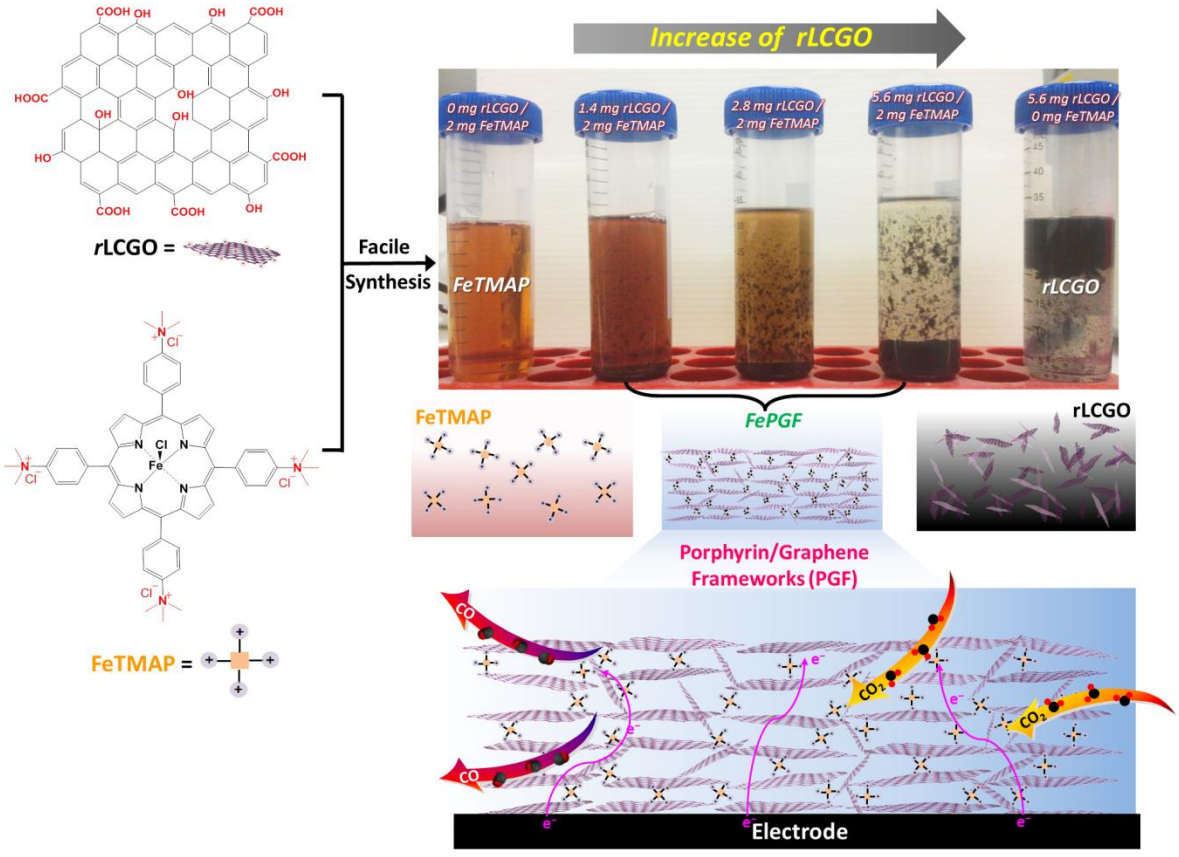

Figure 1. Schematic illustration of the synthesis of FePGF composed of *r*LCGO and FeTMAP, the material characteristics and the electrocatalyst application for the conversion of CO_2 into CO.

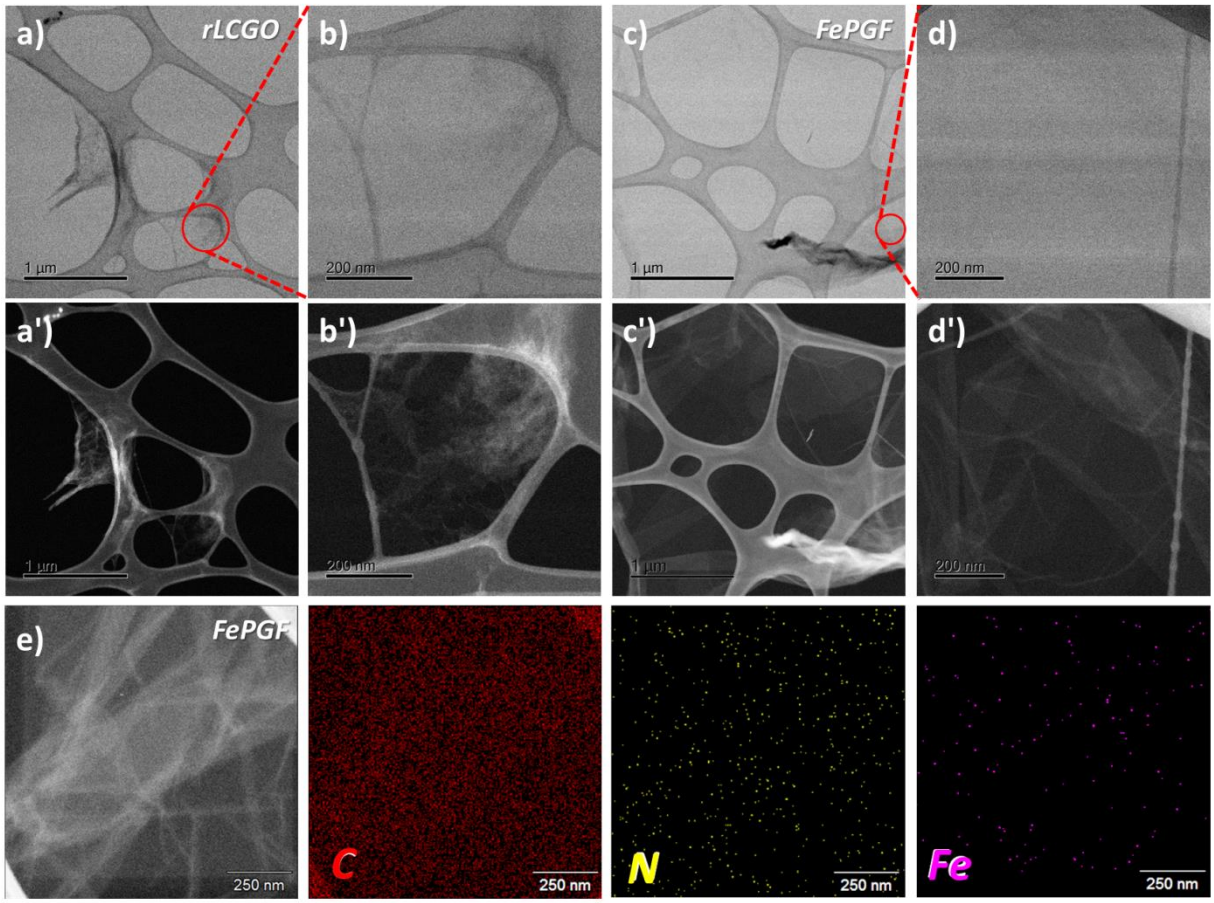

Figure 2. Bright-field TEM images of a) and b) *r*LCGO and c) and d) FePGF, and their corresponding FePGF high-angle annular dark field–scanning TEM (HAADF-STEM) images of a') and b') *r*LCGO and c') and d') FePGF. e) HAADF-STEM image and EDS mappings of the FePGF.

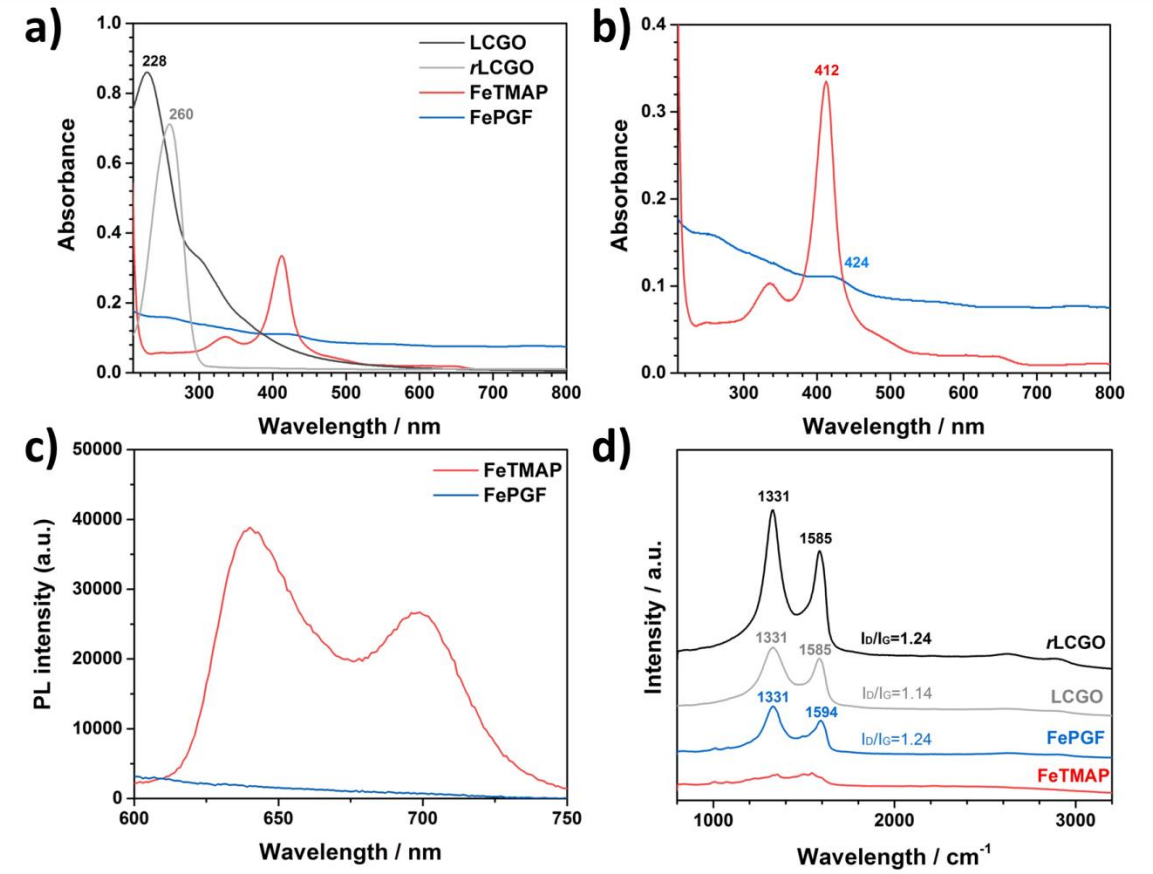

Figure 3. a) UV-Vis absorption spectra of LCGO, *r*LCGO, FeTMAP and FePGF. b) Magnified UV-Vis absorption spectra of FeTMAP and FePGF. c) Fluorescence spectra of FeTMAP (λ_{ex}=412 nm) and FePGF (λ_{ex}=424 nm). d) Raman spectra of LCGO, *r*LCGO, FeTMAP and FePGF.

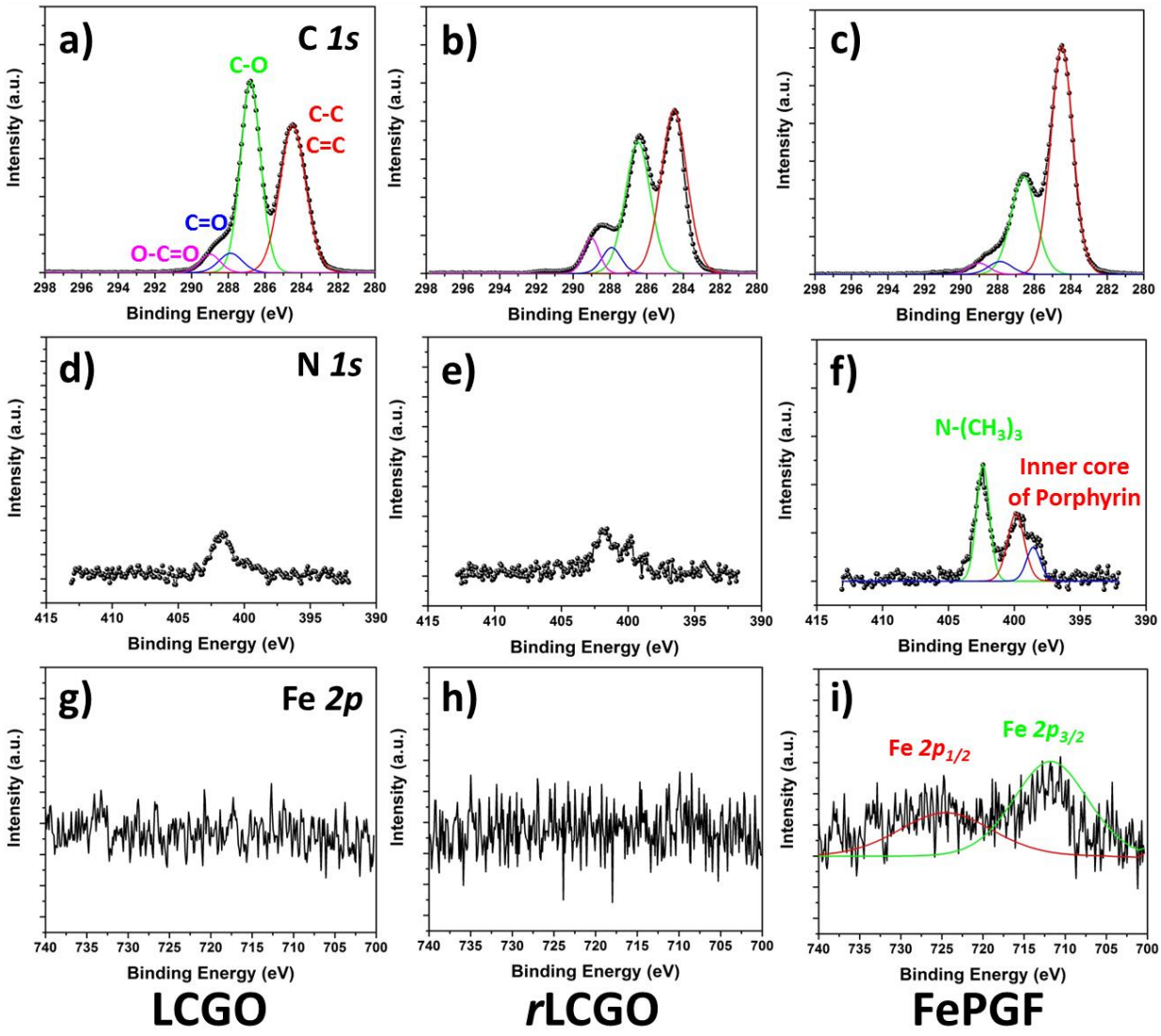

Figure 4. XPS spectra of LCGO, *r*LCGO, and FePGF, respectively, for a-c) C 1s, d-f) N 1s, and g-i) Fe 2p.

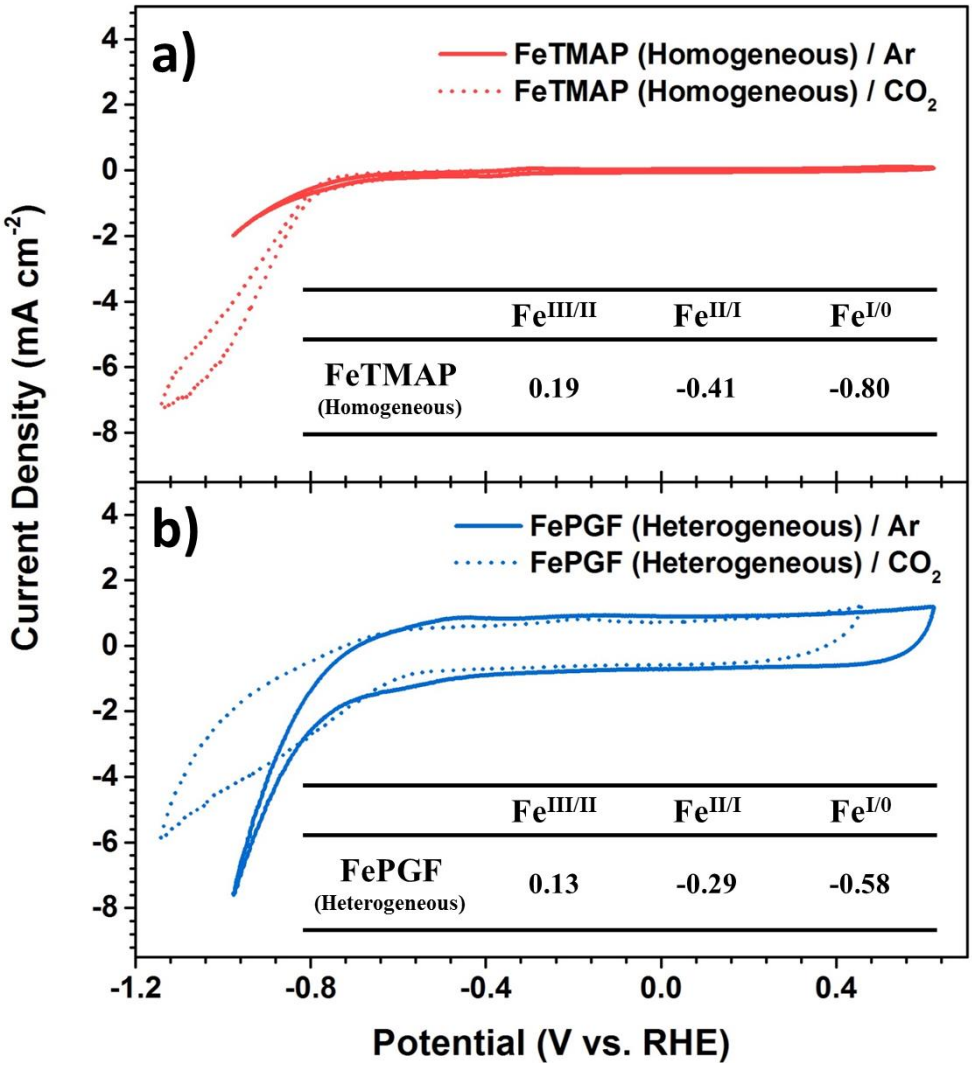

Figure 5. Cyclic voltammograms of a) 0.5 mM FeTMAP-dissolved homogeneous system and b) FePGF as a heterogeneous system in 0.1 M KCl electrolyte. The pH is 7.1 under Ar and 4.2 under CO_2. All scan rates were 100 mV s^{-1}. The inset shows the reduction potentials at the peak of current density of each sample determined by Fourier transform AC cyclic voltammetry (FTACV) in 0.1M KCl electrolyte.

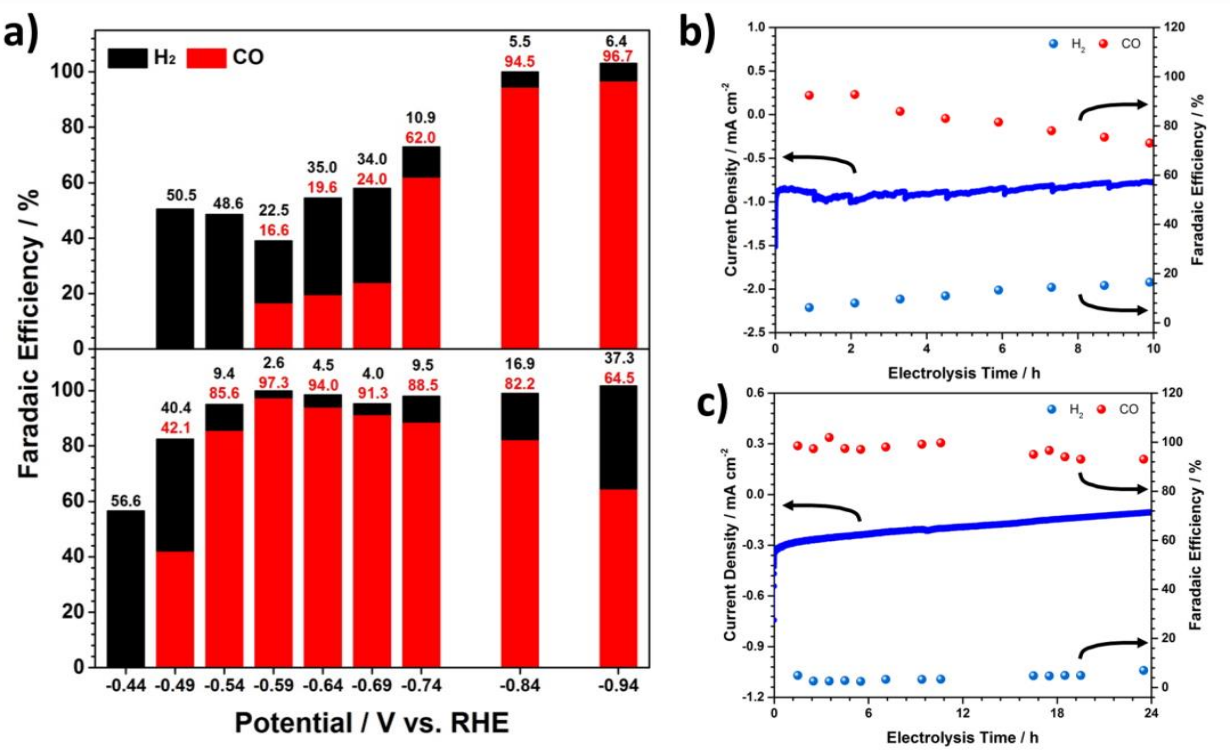

Figure 6. a) Faradaic efficiencies of 0.5 mM FeTMAP as homogeneous catalyst (upper) and FePGF as heterogeneous catalyst (bottom) for CO (red) and H_2 (black) formation at various applied potentials under a CO_2 atmosphere. Long-term stability with respect to current density (blue solid line) and faradaic efficiency (coloured dots) of the CO_2 reduction electrocatalysis by b) 0.5 mM FeTMAP (homogeneous) at -0.84 V for 10 h electrolysis and c) FePGF (heterogeneous) at -0.59 V for 24 h electrolysis in a 0.1 M KCl aqueous electrolyte.

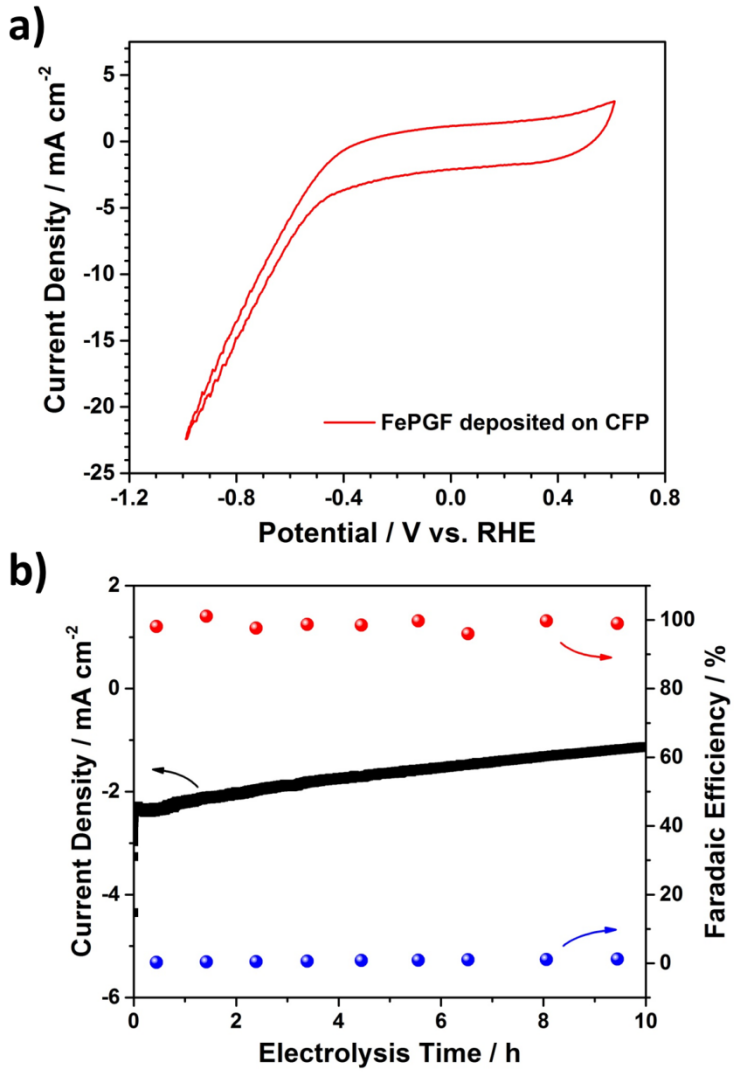

Figure 7. Cyclic voltammogram of FePGF/CFP in CO_2 saturated 0.1 M $KHCO_3$ electrolyte. b) Long-term stability of FePGF/CFP (neutral pH) at -0.54 V (corresponding to an overpotential of 430 mV).

Table 1 Comparison of catalytic activities of FePGF prepared in this study with the state-of-the-art of immobilized molecular complex catalysts for electrochemical CO_2 reduction.

Entry	Catalysts (Electrolysis V vs. RHE[b], pH)	Substrate	Active amount of molecules mol cm^{-2}	Current Density mA cm^{-2}	Faradaic Efficiency for CO/H_2 %	Energy Efficiency[a] %	TOF s^{-1}	TON (Electrolysis time)	Ref.
1	FePGF (-0.54V, pH 6.8)	Carbon fiber paper	3.0×10^{-9}	~ 1.68	98.7% / 0.8%	60.9	2.9	104,400 (10h)	This work
2	FePGF (-0.59V. pH 4.2)	Glassy carbon plate	1.3×10^{-9}	~ 0.20	97.0% / 4.0%	58.5	0.8	69,120 (24h)	This work
3	FePGF (-0.54V, pH 6.8)	Glassy carbon plate	1.3×10^{-9}	~ 0.27	94.2% / 7.1%	58.2	1.0	36,000 (10h)	This work
4	WSCAT/Nafion /Carbon powder[c] (-0.52V, pH 7.3)	Carbon felt	$3.7 – 7.4 \times 10^{-7}$	~ 1.0	90% / 10%	56.1	0.01	1,006 (30h)	[15c]
5	CAT_{pyr}/MWCNT[d] (-0.59V, pH 7.3)	Glassy carbon plate	2.4×10^{-8}	~ 0.20	93% / 4%	56.1	0.04	432 (3h)	[38]
6	CAT_{CO2H}/MWCNT[e] (-0.62V, pH 7.3)	Glassy carbon plate	6.4×10^{-9}	~ 0.16	80% / n.a.	47.6	0.1	1,080 (3h)	[29]
7	CoPc/MWCNT (2.5%)[f] (-0.63V, pH 6.8)	Carbon fiber paper	1.8×10^{-8}	~ 10.0	92% / 6.4%	54.5	2.6	93,600 (10h)	[15e]
8	CoPc-CN/MWCNT (3.5%)[g] (-0.63V, pH 7.2)	Carbon fiber paper	1.8×10^{-8}	~ 15.0	98% / 3.3%	58.1	4.1	14,760 (1h)	[15e]
9	CoTPP/SWCNT[h] (-0.68V, pH 7.2)	Glassy carbon plate	1.7×10^{-7}	~ 3.2	85% / 9%	49.3	0.08	1,194 (4h)	[15d]
10	CoPc-P4VP[i] (-0.73V, pH 4.7)	Edge-plane graphite disc electrode	1.3×10^{-9}	~ 2.0	89% / 5%	50.5	4.8	34,560 (2h)	[39]
11	CoFPc[j] (-0.80V, pH 7.2)	Carbon fiber paper	1.3×10^{-8}	~ 4.5	93% / 5%	51.3	1.61	11,592 (2h)	[40]
12	COF-367-Co (1%)[k] (-0.67V, pH 7.3)	Carbon fiber paper	2.0×10^{-9}	~ 0.45	53% / 62%	30.9	0.62	17,856 (8h)	[15a]

[a] Assuming a 400 mV overpotential for water oxidation at the anode.

[b] All potentials were adjusted to the reversible hydrogen electrode (RHE) using the formulation, E (vs.RHE)=Applied potential (vs.Ag/AgCl)+0.210 V+0.059 V×pH.

[c] 5,10,15,20-Tetrakis(4-trimethylammoniumphenyl)porphyrin-iron(III) pentachloride.

[d] 5,10,15-Tris(2,6-hydroxyphenyl)-20-(3-(pyren-1-yl)propyl)porphyrin-iron(III) chloride.

[e] 5,10,15-Tris(2,6-dihydroxyphenyl)-20-(4-carboxyphenyl)porphyrin-iron(III) chloride.

[f] Cobalt(II) phthalocyanine.

[g] 2,3,9,10,16,17,23,24-Octacyanophthalocyanine-cobalt(II).

[h] 5,10,15,20-Tetraphenylporphyrin-cobalt(II).

[i] Cobalt(II) phthalocyanine-poly-4-vinylpyridine.

[j] 1,2,3,4,8,9,10,11,15,16,17,18,22,23,24,25-Hexadecafluorophthalocyanine-cobalt(II).

[k] 5,10, 15,20-Tetrakis(4-aminophenylporphyrin)-cobalt(II).

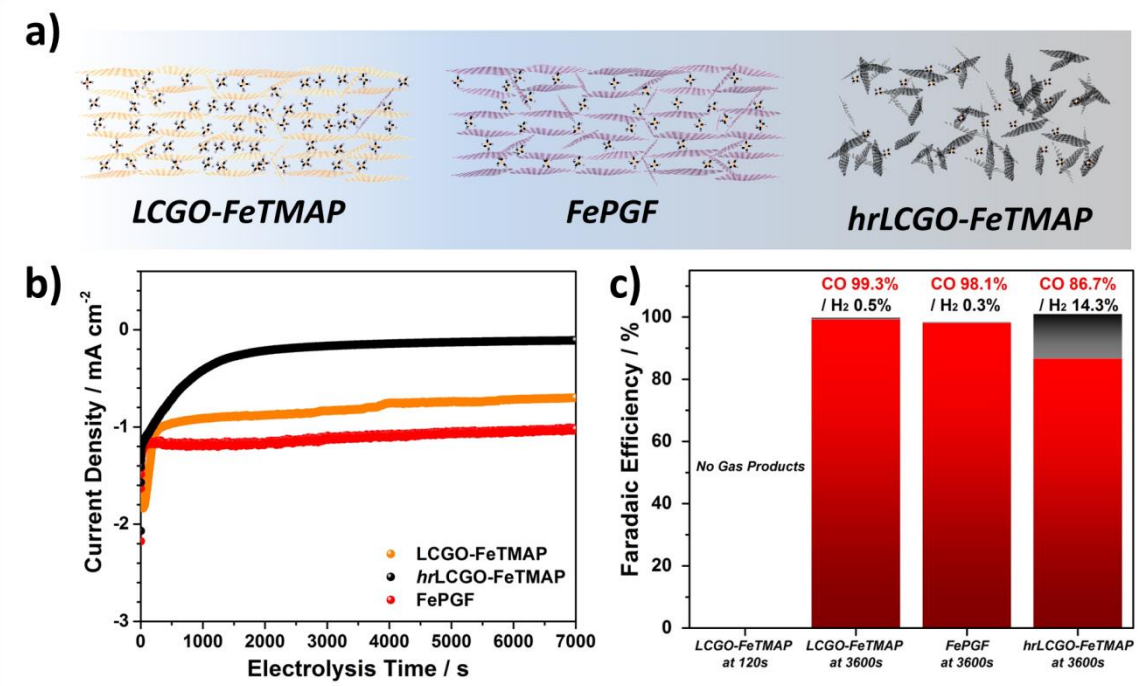

Figure 8. a) Representations of the ideal structures for the LCGO-FeTMAP, FePGF and *hr*LCGO-FeTMAP composites. b) Chronoamperometry of the LCGO-FeTMAP, FePGF and *hr*LCGO-FeTMAP at -0.54 V for 7000 s in 0.1 M $KHCO_3$. c) Faradaic efficiency of the LCGO-FeTMAP, FePGF and *hr*LCGO-FeTMAP catalysis.

A porphyrin-based graphene framework (FePGF) is fabricated *via* a simple and facile self-assembly method for the efficient electrocatalytic reduction of CO_2. FePGF displays an outstandingly robust catalytic performance for the production of CO over 10 to 24 h with 98.7% Faradaic efficiency at an overpotential of 430 mV, corresponding to a TOF of 2.8 s^{-1} and TON of 104,400.

Keyword electrochemical CO_2 reduction, heterogeneous catalyst, water-soluble porphyrin, graphene, framework

Jaecheol Choi, Pawel Wagner, Rouhollah Jalili, Jeonghun Kim, Douglas R. MacFarlane, Gordon G. Wallace*, David L. Officer*

A Porphyrin/Graphene Framework: A Highly Efficient and Robust Electrocatalyst for Carbon Dioxide Reduction

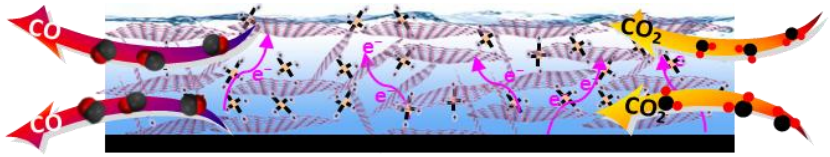

Supporting Information

A Porphyrin/Graphene Framework: A Highly Efficient and Robust Electrocatalyst for Carbon Dioxide Reduction

Jaecheol Choi, Pawel Wagner, Rouhollah Jalili, Jeonghun Kim, Douglas R. MacFarlane, Gordon G. Wallace, and David L. Officer**

1. Experimental section

Apparatus

All chemicals and reagents not described below were commercial and used without further purification. The nuclear magnetic resonance (NMR) spectra were recorded on Varian Avance 500 spectrometer using TMS as an internal standard. Transmission electron microscopic (TEM) images and energy dispersive spectrum (EDS) were collected on a JEOL ARM-200F. UV-Visible spectrum was investigated with a Shimadzu UV-3600 spectrophotometer. Fluorescence was obtained by Horiba Fluorolog FL3-221. Raman spectra were recorded on a Jobin Yvon Horiba HR800 Raman microscope using a 532 nm laser line. Gas chromatography (GC, GC-08, Shimadzu, Japan) was performed with a 6-foot Molecular Sieve 5 Å column and a thermal conductivity detector (TCD). The column was kept at 90°C while the detector was at 100°C. The retention time of each product was compared with known compounds. All the electrochemical experiments were conducted on a CHI 650D electrochemical workstation (CH Instruments, Austin, Texas, USA) at ambient condition.

Synthesis of 5,10,15,20-tetrakis(4-dimethylaminophenyl)-porphyrin

The synthesis was carried out by standard Adler condition using 1:1 mixture of propionic and octanoic acid as the reaction medium[1].

Yield: 12%. The spectral data was comparable to that published previously[2,3].

Synthesis of 5,10,15,20-tetrakis(4-trimethylammoniumphenyl)- porphyrin tetraiodate

5,10,15,20-Tetrakis(4-dimethylaminophenyl)porphyrin (1.78 g, 2.2 mmol) was dissolved in DMF (90 mL) and methyl iodide was added (15 mL, 0.24 mol). The resulting mixture was stirred at 100°C for 5 h then cooled down. The cold mixture was diluted with acetone; resulting solid was filtered off, washed with acetone and diethyl ether then vacuum dried at 60°C to give fine purple powder.

Yield: 77%; 1H NMR (500 MHz, DMSO-d6, TMS): 8.88 (s, 8H, β-pyrrolic), 8.54 – 8.43 (m, 16 H, Ar), 3.96 (s, 24H, N-CH_3), -2.94 (br s, 2H, NH).

Synthesis of 5,10,15,20-tetrakis(4-trimethylammonium-phenyl)porphyrinato iron(III) pentachloride (FeTMAP)

This method was adopted from the procedure presented by Harada *et al.* and modified[4]. 5,10,15,20-Tetrakis(4-trimethylammoniumphenyl)porphyrin tetraiodate (0.63 g, 4.6 mmol) and iron (II) chloride tetrahydrate (46.00 g 0.23 mol) were dissolved in water (250 mL) and refluxed for 2 h in aerobic conditions. The mixture was filtered when hot and the filtrate was cooled down. Sodium perchlorate (10.00 g, 82 mmol) was added to the cold solution and stirred for 15 min then the resulting purple solid was filtered off and washed with 1% perchloric acid. (CAUTION – do not dry the cake. It will explode when dry!). The solid was redissolved in hot acetonitrile (150 mL), cetylpyridinium chloride (8.23 g, 24 mmol) added and the hot mixture stirred for 5 minutes. The resulting solid was filtered off, washed several times with hot acetonitrile then dried under vacuum at 60°C to give FeTMAP as fine dark red microcrystals.

Yield: 97%; The spectral data was comparable to that published previously[5].

Synthesis of *r*LCGO

The experimental setup and procedure for the synthesis of liquid crystalline graphene oxide (LCGO) were based on our previously reported synthesis method[6-8]. Expandable graphite flakes (3772, Asbury Graphite Mills, US) were thermally treated at 1050 °C for 15 s to produce expanded graphite (EG) and this was used as the precursor for graphene oxide synthesis. In a typical GO synthesis, EG (1 g) and sulfuric acid (200 mL) were mixed and stirred in a three-neck flask for 24 h. $KMnO_4$ (5 g) was added to the mixture and stirred at room temperature for 24 h. The mixture was then cooled in an ice bath, and deionized water (200 mL) and H_2O_2 (50 mL) were poured slowly into the mixture, resulting in a colour change to light brown followed by stirring for 30 min. The resulting dispersion was washed and centrifuged three times with a HCl solution (9:1 vol. water/HCl). Repeated centrifugation washing steps with deionized water were carried out until a solution of pH ~6 was achieved. The resulting large GO sheets were redispersed in deionized water by gentle shaking.

The reduction of the LCGO using ascorbic acid was then carried out in deionized (DI) water. Specifically, ascorbic acid (225 mg) was added to a water dispersed LCGO solution (50 mL, 1.5 mg mL^{-1}) and heated at 90°C for 1 h. Upon cooling, the resulting black *r*LCGO was isolated by centrifugation and decantation. The *r*LCGO was redispersed twice with a similar volume of water to wash it and finally redispersed in DI water to give a concentration of 2.8 mg mL^{-1}.

2. Supporting figures and tables

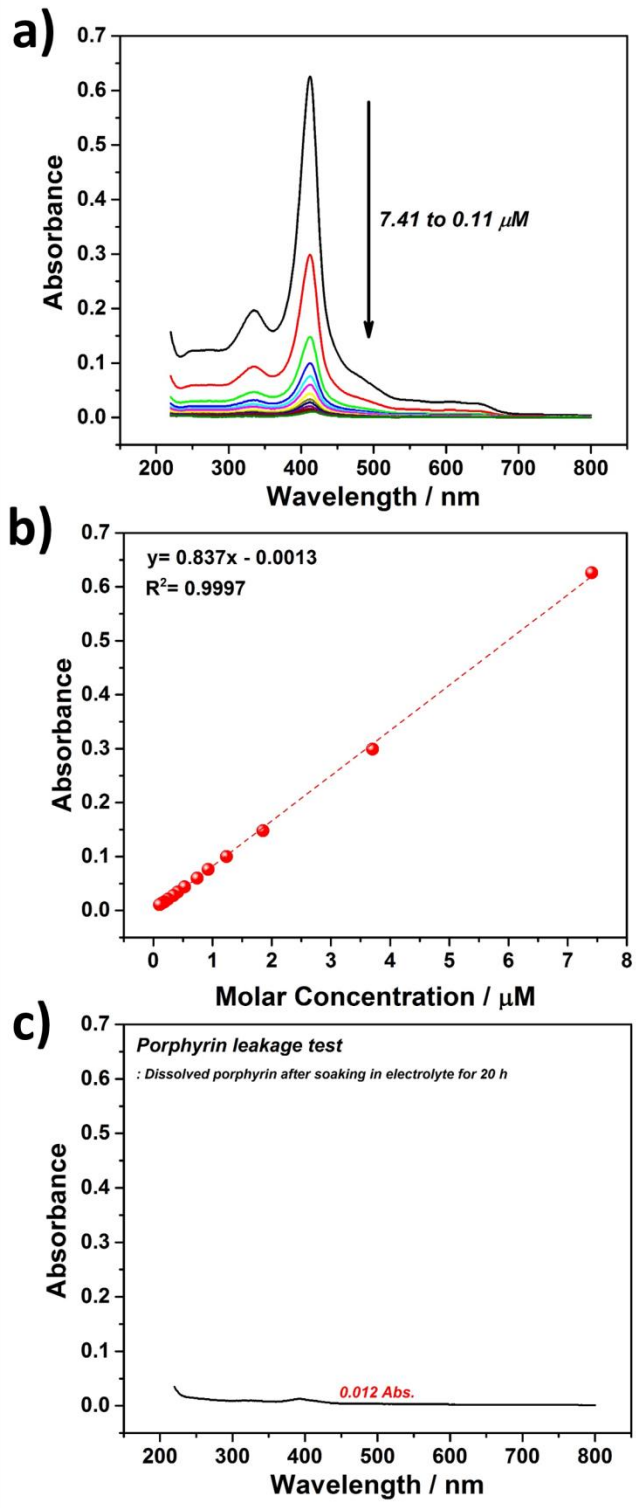

Figure S1 Data obtained to determine the leaching of porphyrin from FePGF. a) UV-Vis spectra of aqueous solutions of FeTMAP at various concentrations from 7.41 to 0.11 μM. b) Calibration curve based on the absorption peaks of the various FeTMAP solutions shown in a). c) UV-Vis spectra of the electrolyte after the immersion of a FePGF electrode for 20 h.

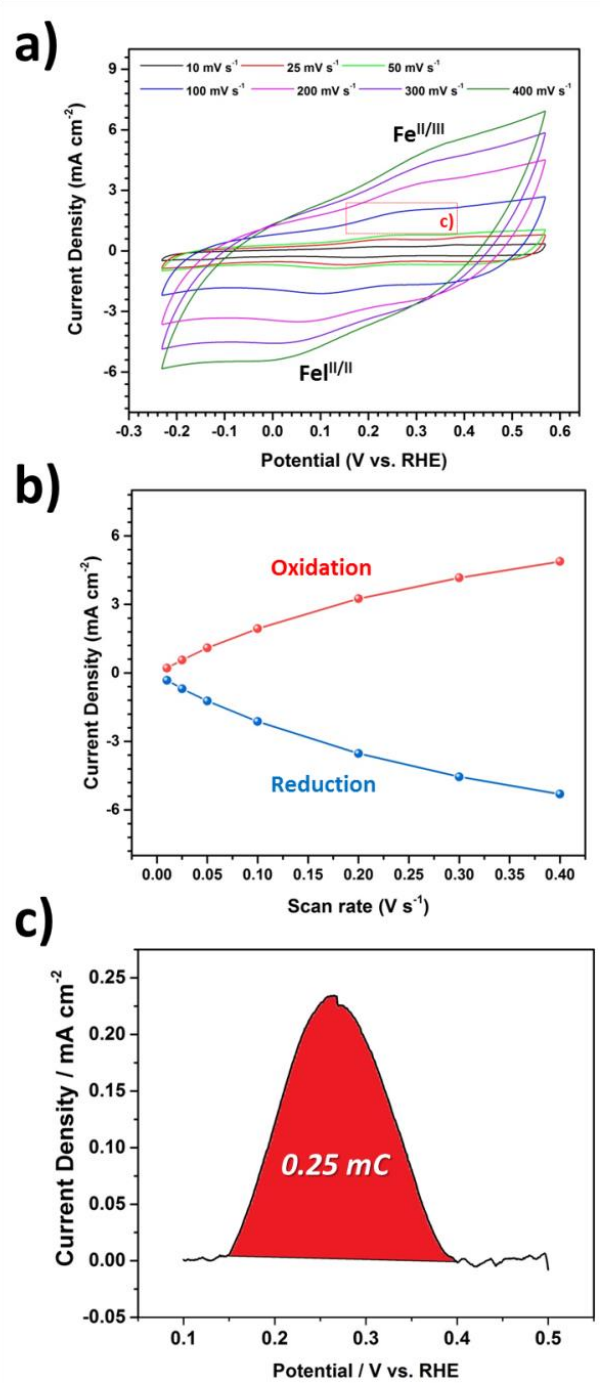

Figure S2 a) Fe^{III}/Fe^{II} redox wave as function of the scan rates in acidic electrolyte (pH 1) brought by adding $HClO_4$ into 0.1 M KCl electrolyte. b) plotting the peak current as a function of the scan rate. c) an example of the integration of the oxidation peak obtained by the red box in Figure S2a.

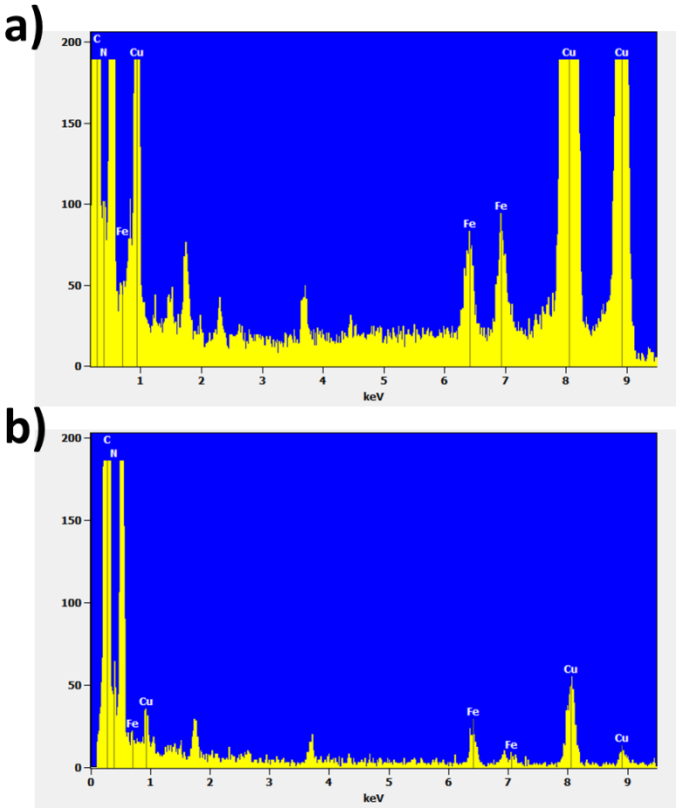

Figure S3 EDS spectra of a) *r*LCGO and b) FePGF.

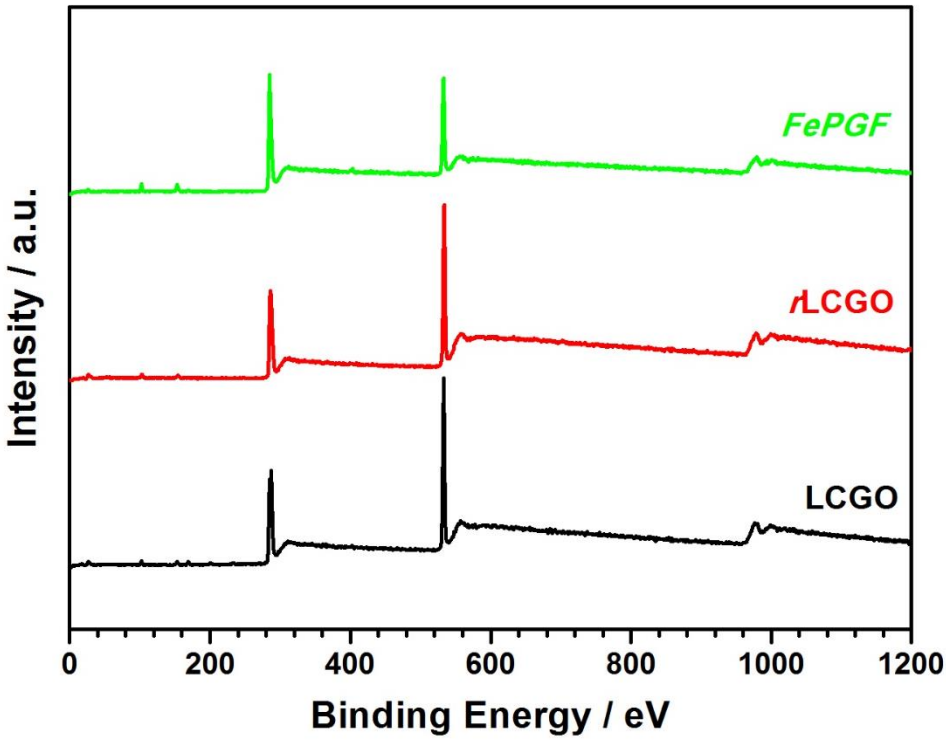

Figure S4 XPS survey spectrum of LCGO, rLCGO and FePGF..

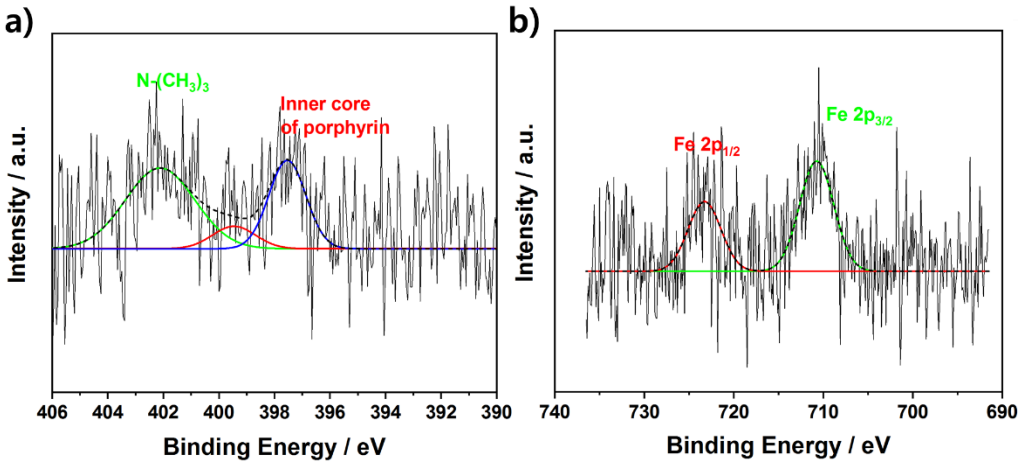

Figure S5 XPS spectra of FeTMAP for a) N 1s and b) Fe 2p.

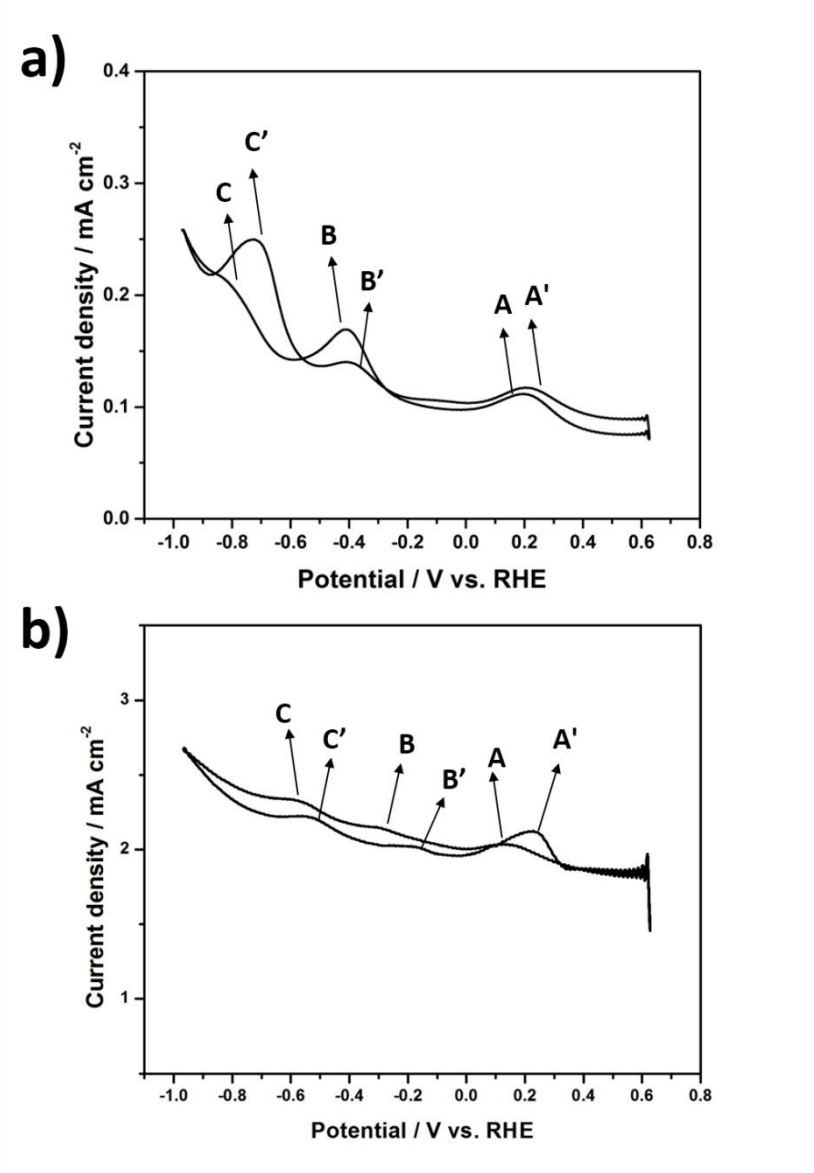

Figure S6 Fourier transform AC voltammograms (FTACV) to determine the redox potentials of Fe in a) homogeneous FeTMAP and b) heterogeneous FePGF. Reduction: A = Fe^{III}/Fe^{II}, B = Fe^{II}/Fe^{I}, C = Fe^{I}/Fe^{0}. Oxidation: A' = Fe^{II}/Fe^{III}, B' = Fe^{I}/Fe^{II}, C' = Fe^{0}/Fe^{I}.

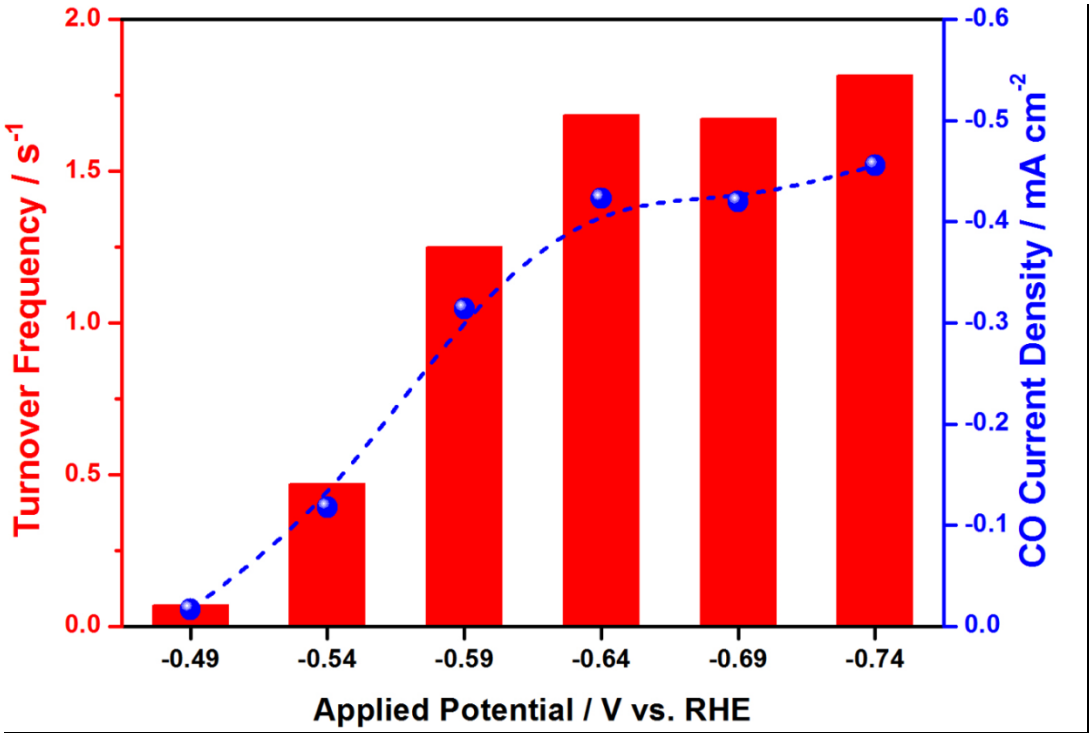

Figure S7 TOF for CO production with FePGF for 20 min electrolysis at different applied potentials.

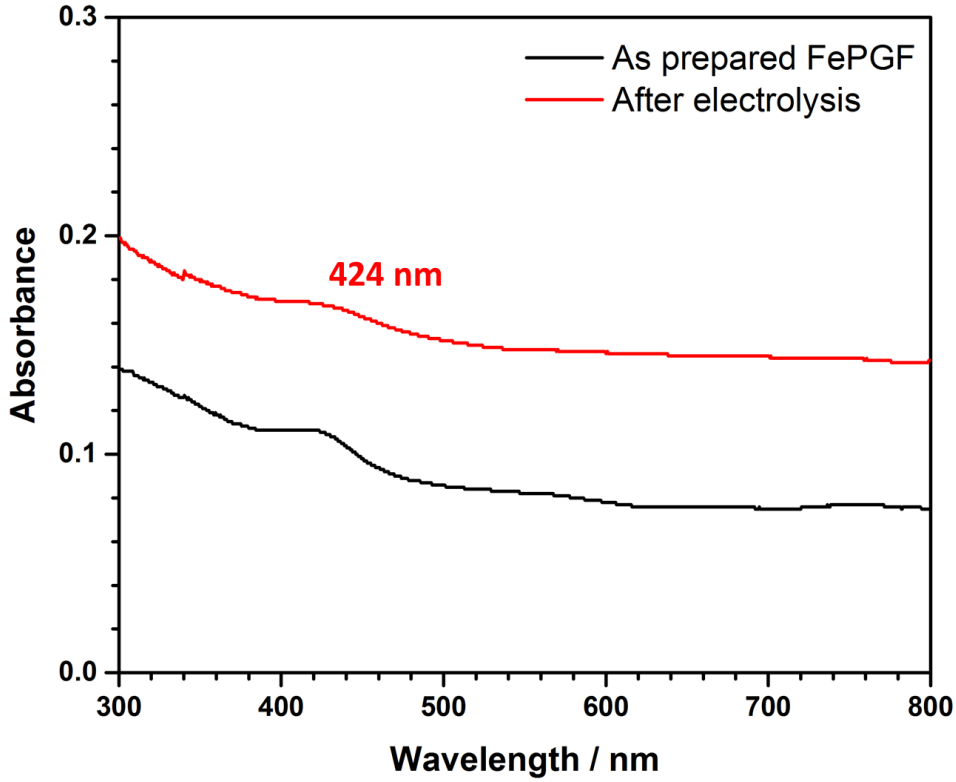

Figure S8 UV-Vis spectrum of FePGF after 24 h electrolysis in 0.1 M KCl electrolyte.

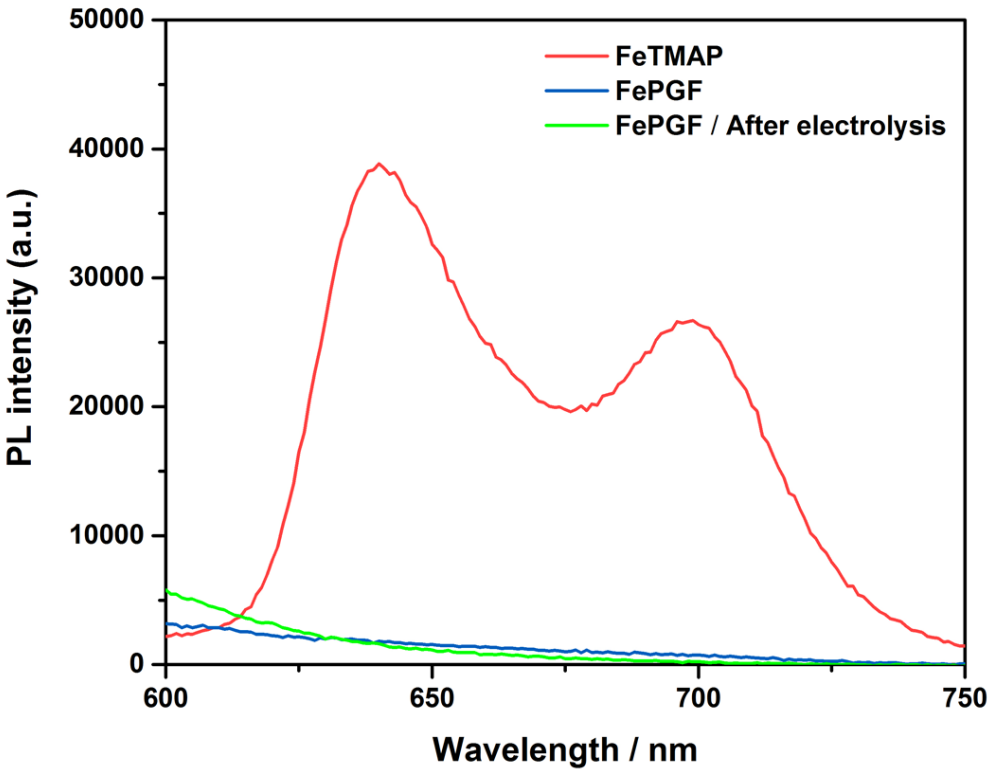

Figure S9 Fluorescence spectra of FeTMAP (λ_{ex}=412 nm), FePGF (λ_{ex}=424 nm) and FePGF after 24 h electrolysis (λ_{ex}=424 nm).

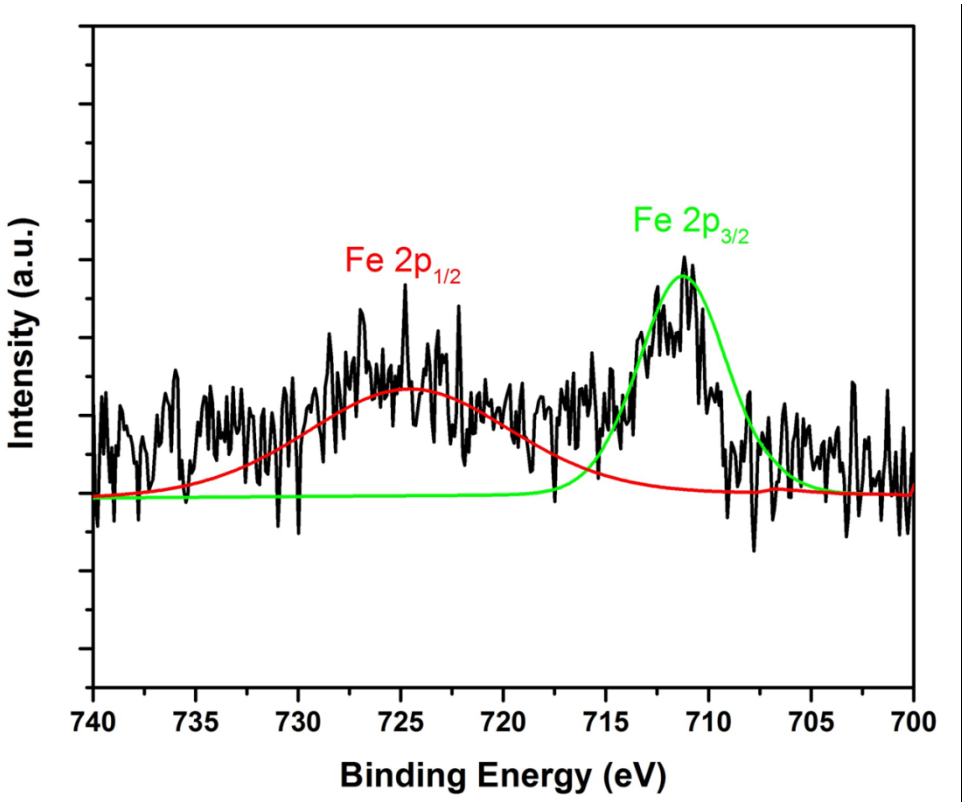

Figure S10 High resolution Fe 2p XPS spectra of FePGF after 24 h electrolysis in 0.1M KCl electrolyte.

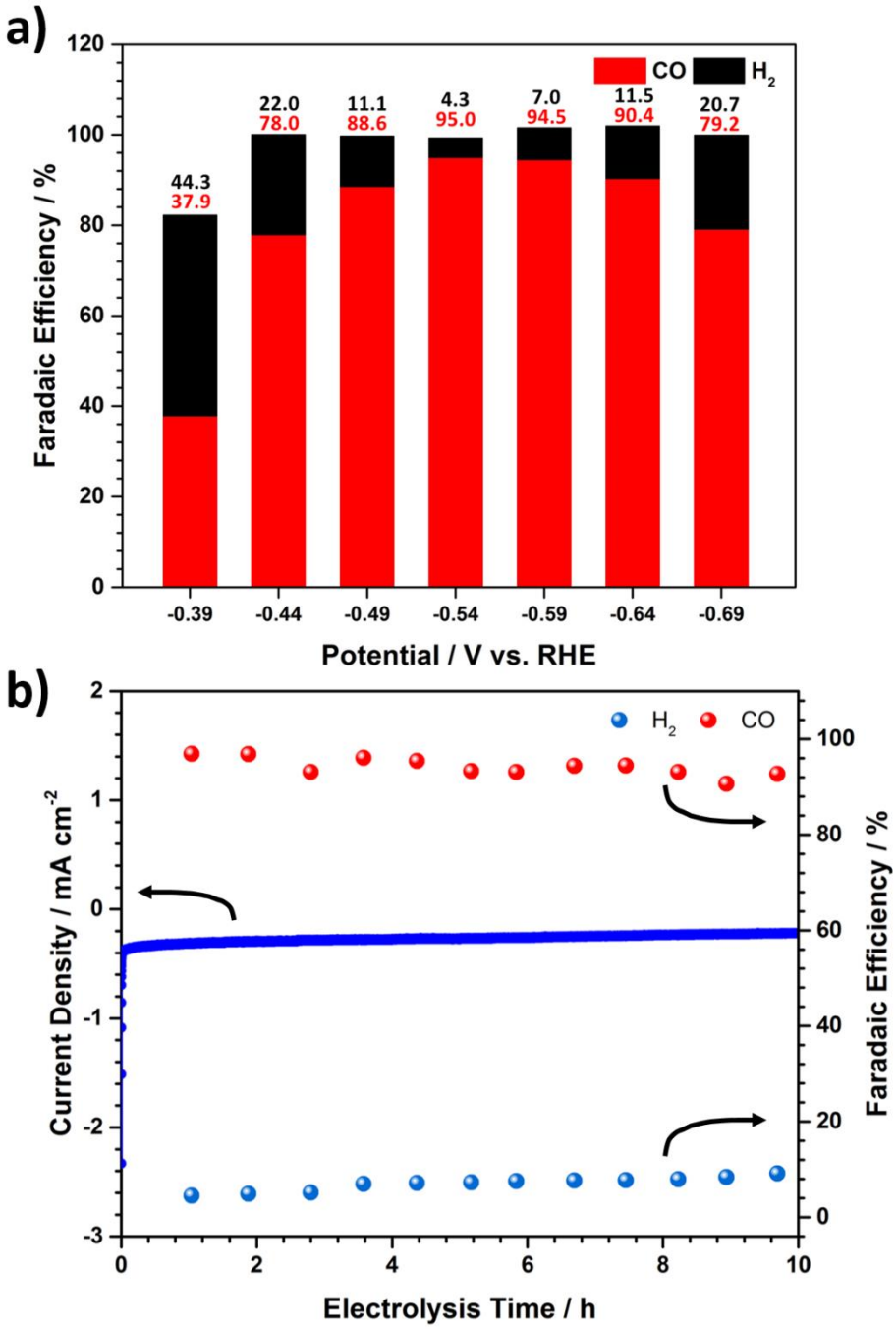

Figure S11 a) Faradaic efficiencies of FePGF for CO/H_2 at various applied potentials at neutral pH (6.8) (CO: red, H_2: black). b) Long-term stability of FePGF (neutral pH) at -0.54 V (corresponding to an overpotential of 430 mV).

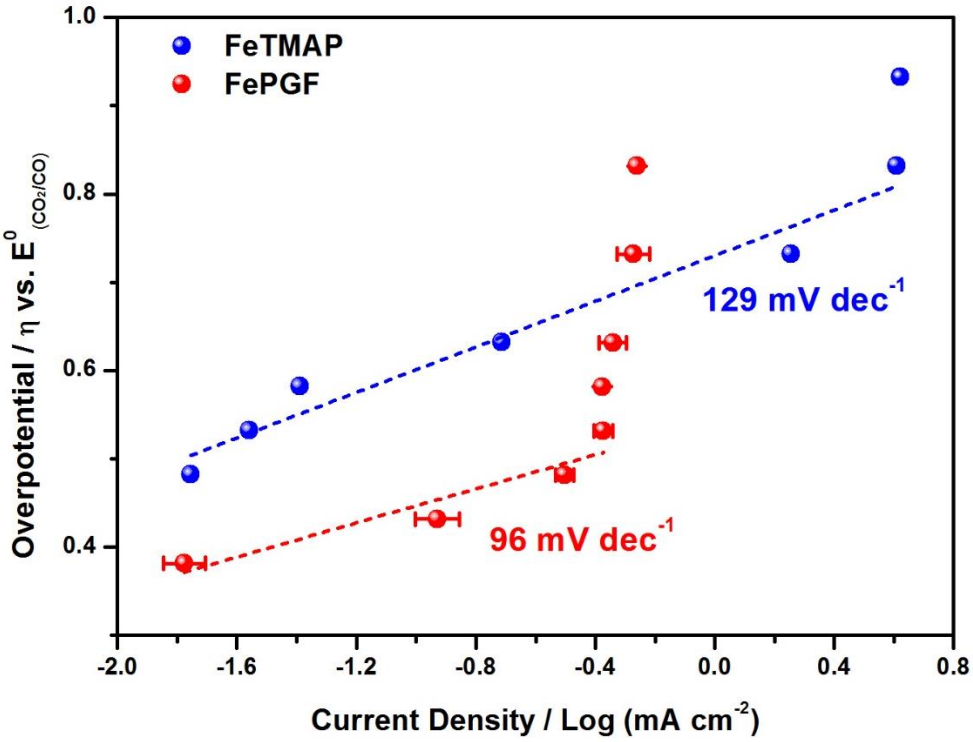

Figure S12 Tafel plots of FePGF (red) and 0.5 mM FeTMAP (blue) for CO production.

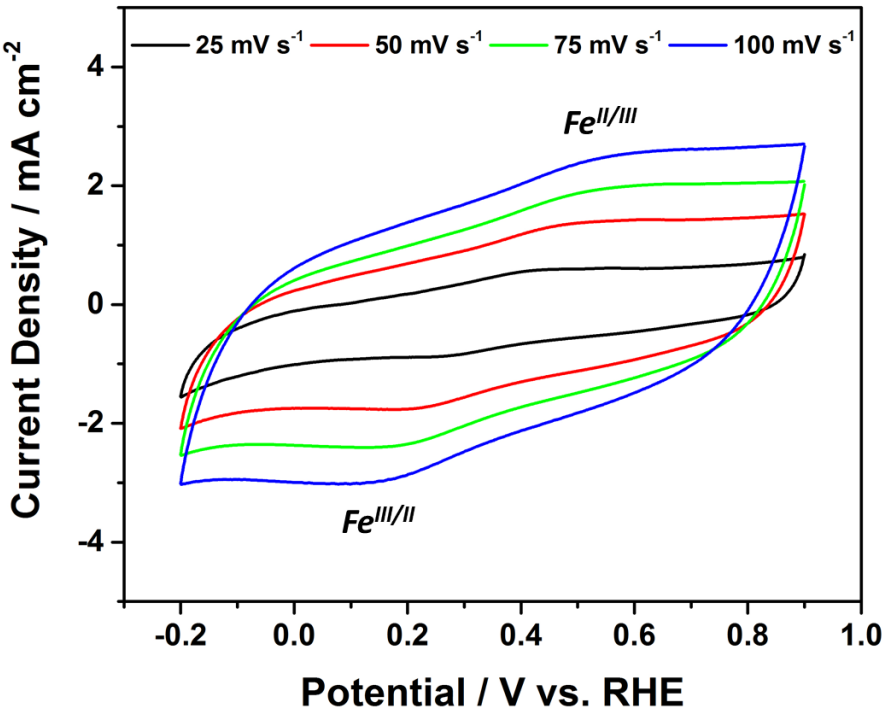

Figure S13 Fe^{III}/Fe^{II} redox wave of the FePGF/CFP electrode as function of the scan rates in Ar-saturated 0.1M $KHCO_3$ (pH 8.3).

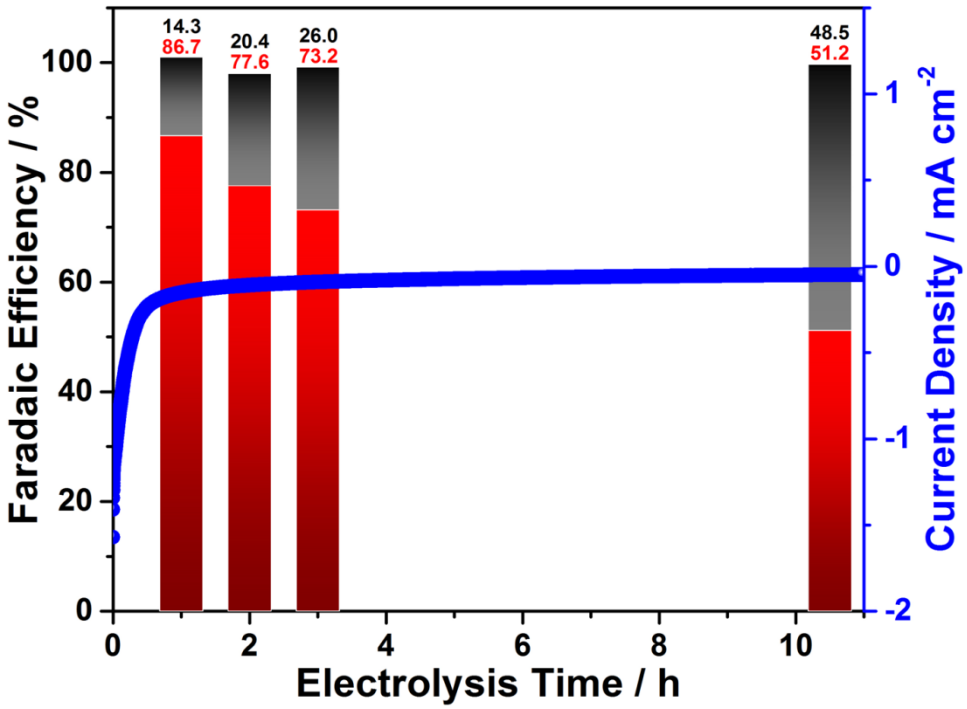

Figure S14 Long-term stability of *hr*LCGO-FeTMAP (neutral pH) at -0.54 V (corresponding to an overpotential of 430 mV) with faradaic efficiencies for CO/H_2 (CO: red, H_2: black).

Table S1 The atomic percentages of each C 1s peak for LCGO, *r*LCGO and FePGF.

	LCGO		*r*LCGO		FePGF	
	Binding energy (eV)	Atomic %	Binding energy (eV)	Atomic %	Binding energy (eV)	Atomic %
C=C/C-C	284.5	45.0	284.5	49.2	284.5	63.0
C-O	286	45.4	286	38.7	286	30.7
C=O	287	5.3	287	5.7	287	3.6
O=C-O	290	4.3	290	6.4	290	2.7

Note S1 Calculation of the number of active FeTMAP molecules on the framework surface

The number of added FeTMAP molecules in the electrode sample

Mole of added porphyrins in the electrode sample

$$= \frac{\boldsymbol{weight\ of\ FeTMAP\ (g)}}{\boldsymbol{molecular\ weight\ (g\ mol^{-1})}}$$

$$= \frac{\mathbf{0.00008}\ \boldsymbol{g}}{\mathbf{1075}\ \boldsymbol{g\ mol^{-1}}} = \mathbf{7.44 \times 10^{-8}\ mol}$$

The number of added porphyrins in the electrode sample

$$= \textbf{Mole of added porphyrins in the electrode sample (mol)} \times \boldsymbol{Avogadro's\ number\ (mol^{-1})}$$

$$= \mathbf{7.44 \times 10^{-8}\ mol} \times \mathbf{6.02 \times 10^{23}}\ \boldsymbol{mol^{-1}} = \mathbf{4.48 \times 10^{16}}$$

The number of active FeTMAP molecules on the framework surface

The number of active porphyrins on framework

$$= \textbf{Mole of active porphyrins on framework (mol cm}^{-2}\textbf{)} \times \boldsymbol{electrode\ area\ (cm^2)} \times \boldsymbol{Avogadro's\ number\ (mol^{-1})}$$

$$= \mathbf{2.6 \times 10^{-9}mol} \times \mathbf{6.02 \times 10^{23}}\ \boldsymbol{mol^{-1}} = \mathbf{1.56 \times 10^{15}}$$

Note S2 Calculation of turnover frequency (TOF) and turnover number (TON)

A. FePGF/Glassy carbon electrode long-term electrolysis at -0.59V

Turnover frequency (TOF)

$$\textbf{TOF}\ (s^{-1}) = \frac{I \cdot FE}{2 \cdot F \cdot n}$$

I : The average current density obtained by 24 h electrolysis at -0.59V (0.00020 A cm^{-2} × 2 cm^2 = 0.00040 A)

FE : The average CO Faradaic efficiency obtained by 24 h electrolysis (97.0%)

F: Faraday constant (96485 C mol^{-1})

n: The amount of catalysts utilized for catalysis (1.3×10^{-9} mol cm^{-2} × 2 cm^2 = 2.6×10^{-9} mol)

$$\textbf{TOF}\ (s^{-1}) = \frac{0.00040A \cdot 0.970}{2 \cdot 96485\ C\ mol^{-1} \cdot 2.6 \times 10^{-9} mol} = 0.8\ s^{-1}$$

Turnover number (TON)

$$\textbf{TON} = \textbf{TOF}\ (s^{-1}) \times \textbf{Electrolysis time}\ (\textbf{s})$$

$$\textbf{TON} = 0.8\ s^{-1} \times 86,400\ \textbf{s} = 69,120$$

B. FePGF/Carbon fiber paper long-term electrolysis at -0.54 V

Turnover frequency (TOF)

$$\textbf{TOF}\ (s^{-1}) = \frac{I \cdot FE}{2 \cdot F \cdot n}$$

I : The average current density obtained by 10 h electrolysis at -0.54V (0.00168 A cm^{-2} × 1 cm^2 = 0.00168 A)

FE : The average CO Faradaic efficiency obtained by 10 h electrolysis (98.7%)

F: Faraday constant (96485 C mol^{-1})

n: The amount of catalysts utilized for catalysis (3.0×10^{-9} mol cm^{-2} × 1 cm^2 = 3.0×10^{-9} mol)

$$\textbf{TOF}\ (s^{-1}) = \frac{0.00168A \cdot 0.987}{2 \cdot 96485\ C\ mol^{-1} \cdot 3.0 \times 10^{-9} mol} = 2.9\ s^{-1}$$

Turnover number (TON)

$$\textbf{TON} = \textbf{TOF}\ (s^{-1}) \times \textbf{Electrolysis time}\ (\textbf{s})$$

$$\textbf{TON} = 2.9\ s^{-1} \times 36,000\ \textbf{s} = 104,400$$

3. References

(1) Adler, A. D.; Longo, F. R.; Finarelli, J. D.; Goldmacher, J.; Assour, J.; Korsakoff, L. *J. Org. Chem.* **1967**, *32*, 476.

(2) Datta-Gupta, N.; Bardos, T. *J. Heterocycl. Chem.* **1966**, *3*, 495.

(3) Walter, R. I.; Ojadi, E. C.; Linschitz, H. *J. Phys. Chem.* **1993**, *97*, 13308.

(4) Yamaguchi, H.; Tsubouchi, K.; Kawaguchi, K.; Horita, E.; Harada, A. *Chem. - Eur. J.* **2004**, *10*, 6179.

(5) Rahiman, A. K.; Bharathi, K. S.; Sreedaran, S.; Narayanan, V. *Catal. Letters* **2009**, *127*, 175.

(6) Jalili, R.; Aboutalebi, S. H.; Esrafilzadeh, D.; Konstantinov, K.; Moulton, S. E.; Razal, J. M.; Wallace, G. G. *ACS Nano* **2013**, *7*, 3981.

(7) Kim, J. E.; Han, T. H.; Lee, S. H.; Kim, J. Y.; Ahn, C. W.; Yun, J. M.; Kim, S. O. *Angew. Chem., Int. Ed.* **2011**, *50*, 3043.

(8) Jalili, R.; Aboutalebi, S. H.; Esrafilzadeh, D.; Konstantinov, K.; Razal, J. M.; Moulton, S. E.; Wallace, G. G. *Mater. Horiz* **2014**, *1*, 87.